國 立 交 通 大 學

顯示科技研究所

碩 士 論 文

量子點面射型雷射高頻特性之研究

High Speed Characteristics of Quantum Dot
Vertical Cavity Surface-Emitting Laser

研 究 生：蔡文凱

指導教授：郭浩中　教授

中 華 民 國 九 十 五 年 七 月

1

量子點面射型雷射高頻特性之研究

High Speed Characteristics of Quantum Dot Vertical Cavity
Surface-Emitting Laser

研 究 生：蔡文凱　　　　　Student：Wen-Kai Tsai

指導教授：郭浩中　　　　　Advisor：Hao-Chung Kuo

國 立 交 通 大 學
顯示科技研究所
碩 士 論 文

A Thesis
Submitted to Institute of Electronics College of Engineering
National Chiao Tung University
in partial Fulfillment of the Requirements
for the Degree of
Master
in

Electo-Optical Engineering

July 2006

Hsinchu, Taiwan, Republic of China

中華民國九十五年七月

量子點面射型雷射高頻特性之研究

研究生：蔡文凱　　　　　　　　　　指導教授：郭浩中教授

國立交通大學顯示科技研究所

摘要

　　本論文旨在研究量子點面射型雷射以及其動態特性的分析。論文分為三個部分，第一個部分，我們提出從雷射的直流特性，包括 LIV 曲線、發光頻譜圖及其變溫特性。此外也展示此量子點雷射的高頻特性，且展示了 2.5Gb/s 的眼圖。論文的第二部分，則是利用外部注入鎖定(injection locking)的技術，來改善雷射的高頻特性，包括增進雷射的小信號頻寬，從原本的 1.7GHz 提升到 7.2GHz，並且在 7GHz 的頻帶載入 50Mb/s 信號，可以觀測出一個清晰的眼圖。此外，利用注入鎖定技術，可以改善雷射的諧波失真項的特性，從 100MHz~1.4GHz 都能改善 10dB 以上。論文的最後，則是利用量子點面射型雷射來當作延遲光行進速度的元件，隨著偏壓電流的不同，可以形成不同延遲的效果，在 10GHz 的操作之下，可以達到 42ps 的延遲，我們同時也針對不同輸入信號強度以及不同頻率下的操作，來觀測其延遲的情形。

High Speed Characteristics of Quantum Dot Vertical Cavity Surface Emitting Laser

Student：Wen-Kai Tsai   Advisor：Prof. Hao-Chung Kuo

Display Institute
National Chiao Tung University

Abstract

The thesis studies the fabrication, measurements and the high speed characteristics of quantum dots vertical cavity surface-emitting laser (QD VCSEL). This thesis can be divided into three parts. In the first parts, we present monolithic QD VCSELs operating in the 1.3 μm optical communication wavelength. The QD VCSELs have adapted fully doped structure on GaAs substrate. The output power is ~ 330 μW with slope efficiency of 0.18 W/A at room temperature. Single mode operation was obtained with side-mode suppression ratio of > 30 dB. Modulation bandwidth and eye diagram in 2.5 Gb/s was also presented. In the second part of this thesis, we report the dynamic characteristics of 1.3μm QD VCSEL without and with light injection. The 3 dB frequency response of QD VCSEL based on TO-Can package is enhanced from the free-running 1.75 GHz to 7.44 GHz with the light injection technique. We also report the second harmonic distortion of QD VCSEL with and without external light injection. We observed that the second harmonic distortion of the QD VCSEL with light injection has been suppressed by more than 14 dB. A 50 Mb/s non-return-to-zero (NRZ) pseudo-random binary sequence (PRBS) data with $2^{31} - 1$ pattern length from a pattern generator is mixed with a 7 GHz RF carrier and then used to directly modulate the QD VCSEL. The QD VCSEL without light injection cannot generate 7-GHz 50-Mb/s data due to the limited frequency response. With light injection technique, the corresponding eye diagrams can be clearly observed. At the end of this thesis, we experimentally demonstrate tunable slow light in an 1.3 μm QD VCSEL at 10 GHz. Tunable optical group delays are achieved by varying the bias currents, and the maximum delay of 42 ps at 10 GHz has been demonstrated at room temperature.

Contents

List of figures

Chapter 2

Chapter 3

Chapter 4

Chapter 1 Introduction

1.1 Introduction of Quantum Dot VCSEL

Vertical-cavity surface-emitting lasers (VCSELs) at around 1.3 μm fabricated on GaAs substrates have been expected to realize high-performance and low-cost light sources for fiber-optic communication systems. The large conduction band offset improves the temperature performance over that of conventional InP-based materials. The GaAs system provides high-performance AlGaAs/GaAs DBR mirrors and permits the use of the well-established oxide-confined GaAs-based VCSEL manufacturing infrastructure. So far, the most promising materials at 1.3 μm on GaAs substrate were GaInAsN quantum wells (QWs) [1-3] and quantum dots (QDs) [4-6]. Each of these solutions offers some advantages over its counterpart, but further extend the emission wavelength is relatively easy in quantum dots than GaInAsN. QDs edge-emitting lasers have also been proven to exhibit excellent performance characteristics, including low threshold current, temperature insensitive threshold current, and high differential gain. For VCSELs, QDs [7] are particularly advantageous, as nonequilibrium carriers are localized in the QDs and thus spreading of nonequilibrium carriers out of the injection region can be suppressed. This may result in ultralow threshold currents at ultrasmall apertures [7-8].

1.2 Review of Injection Locking technique

Since the early 1980s, the research topic injection locking of semiconductor lasers has attracted much interest. Its applications include receiver end design in optical coherent communication[9], laser spectral narrowing[10], suppression of laser noise[11], the reduction of frequency chirp under modulation[12], and improving the laser intrinsic frequency response[13].

For digital communication, the high-linewidth enhancement factor leads to high chirp that is undesirable. In analog fiber-optic transmission systems have many applications such as CATV and fiber radio systems. [14] In these applications, the direct modulation of semiconductor lasers can be used for transmitting subcarrier-multiplexed signals at low cost. However, when semiconductor lasers are directly modulated, nonlinear distortions occur. In the low frequency applications, nonlinear light-vensus-current characteristics are the main cause of distortions. For direct modulation with RF-range

frequency, the nonlinearity resulting from the coupling between photons and electrons in the laser cavity is dominant. This coupling also results in the relaxation oscillation resonance. Such distortions can cause severe system performance degradation, because they cause inter-channel interference that limits the number of channels as well as transmission distance. For the highest capacity systems, designers typically have chosen to incorporate an external modulation device to a continuous-wave laser. Though this may achieve the desired performance requirements, it does so with the cost of additional system complexity. If possible, a directly modulated laser with higher performance would be ideal. Injection Locking can increase the laser relaxation oscillation frequency, which causes the intrinsic nonlinear distortion suppression in directly modulated semiconductor lasers and gives us the additional design freedom with greatly increased performance that makes injection-locked directly modulated lasers a viable candidate for future analog and digital networks.

1.3 Review of Slow Light

In optical communication, a controllable variable optical buffer is one of the most critical components. In such buffer, optical data would be kept in optical format throughout the storage time without being converted into electronic format. The turn-on and turn-off time should be variable with an external control. The most important application of optical buffers is perhaps all-optical routers in packet-switched networks. A router is used in networks to interconnect end-user systems to each other where packets are the basic units of information that are transported. A router often connects many networks and performs decisions on how to send packets from its source to its destination in the network. Packet switching is a method of communication whereby information is broken up into blocks of limited length called packets. They are then switched in a network by routers. The key building blocks of an electronic router include a switch fabric, processors, and buffers. The key missing component for an all-optical router is an all-optical buffer. With optical buffers, one packet can be stored in the buffer temporarily, allowing the other packet to go first. Until the traffic is cleared at the output port, the packet stored in the buffer is released. An all-optical router can potentially alleviate the traffic congestion in future very-high-bandwidth networks. However, variable optical delay lines (also called "slow light" devices) and buffers will be crucial components in

optical communication, phased array antenna, and signal processing systems. There are several technical approaches to implement an optical buffer. No matter what methods, the medium which the optical signal travels in should be varied by either increasing the path length or reducing the signal group velocity. The former can be achieved by using of a fiber delay line or resonant cavity and the latter has several possibilities, such as EIT, CPO. Recently, tunable slow light using an InGaAsP quantum well Fabry-Perot laser has been reported [15]. Tunable optical group delays 14 ps for 2 GHz sinusoidal signal have been demonstrated, and the delay-bandwidth product was 0.028. Moreover, tunable slow light using a quantum well VCSEL fabricated on InP-based materials also has been proposed [16]. The modulation frequency of probe signal between 1-3 GHz was presented, and the delay-bandwidth product was 0.28 (100 ps × 2.8 GHz).

1.4 Organization of the thesis

This thesis consists of three related parts. In Chapter 2, we demonstrate monolithically single-mode QD VCSELs with high side-mode suppression ratio (> 30 dB) and report the temperature performance and dynamic properties including bandwidth and eye diagram.

In Chapter 3, we report the experimental characterization of 1.3μm QD VCSEL with and without external light injection. Significant frequency response enhancement has been observed. Furthermore, we demonstrate that this frequency response enhancement allows us to improve the performance of subcarrier multiplexed (SCM) system. We also report the third-order intermodulation distortion (IMD3) of QD VCSEL with and without external light injection.

In Chapter 4, we report the slow light in the monolithically single-mode QD VCSEL. Tunable optical group delay can be achieved by adjusting the bias current. A 10 GHz modulation signal with tunable optical group delays 42 ps has been demonstrated. We also study the relationship between the signal input power and the tunable optical group delay. Finally, summary of research results will be given in Chapter 5. Suggestion for future work is also presented.

Reference

[1] N. Tansu and L. J. Mawst, "Temperature sensitivity of 1300-nm InGaAsN quantum-well lasers", *IEEE Photonics Technology Letters,* vol. 14, no. 8, pp. 1052-1054, 2002.

[2] C. W. Tu and Pkl Yu, "Material properties of III-V semiconductors for lasers and detectors," *MRS Bulletin*, vol. 28, pp. 345-349, 2003.

[3] M. Kawaguchi, T. Miyamoto, E. Gouardes, D. Schlenker, T. Kondo, F. Koyama and K. Iga "Lasing Characteristics of Low-Threshold GaInNAs Lasers Grown by Metalorganic Chemical Vapor Deposition,"*Japanese Journal of Applied Physics*, vol. 40, pp. L744–L746, 2001.

[4] S. L. Chuang, N. Holonyak, Jr. "Quantum-well assisted tunneling injection quantum-dot lasers," *Conference on Lasers and Electro-Optics, Technical Digest*, vol. 1, pp. 297, 2002.

[5] T. Yang, J. Tatebayashi, S. Tsukamoto and Y. Arakawa," Highly uniform self-assembled InAs/GaAs quantum dots emitting at 1.3μm by metalorganic chemical vapor deposition," *Physica E*, vol. 26, pp. 77-80, 2005.

[6] N. N. Ledentsov, "Long-wavelength quantum-dot lasers on GaAs substrates: from media to device concepts," *IEEE Journal of Selected Topics in Quantum Electronics*, vol. 8, pp. 1015 - 1024, 2002.

[7] N. N. Ledentsov, M. Grundmann, F. Heinrichsdor, D. Bimberg, V.M. Ustinov, A. E. Zhukov, M. V. Maximov, Zh. I. Alferov, J. A. Lott, "Quantum-Dot Heterostructure Lasers," *IEEE Journal of Selected Topics in Quantum Electronics*, vol. 6, no. 3, pp. 439-451, 2000.

[8] J. A. Lott, N. N. Ledentsov, V. M. Ustinov, A. Yu. Egorov, A. E. Zhukov, P. S. Kop'ev, Zh. I. Alferov, and D. Bimberg, "Vertical cavity lasers based on vertically coupled quantum dots," *Electronics Letters*, vol. 33, pp. 1150-1151, 1997.

[9] Y. Yamamoto and T. Kimura, "Coherent optical fiber transmission systems,"*IEEE J. Quantum Electron.*, vol. QE-17, pp. 919–935, June 1981.

[10] P. Gallion, H. Nakajima, G. Debarge, and C. Chabran, "Contribution ofspontaneous emission to the linewidth of an injection-locked semiconductorlaser," *Electron. Lett.*, vol. 22, pp. 626–628, 1985.

[11] K. Iwashita and K. Nakagawa, "Suppression of mode partition noise by laser diode light injection," *IEEE J. Quantum Electron.*, vol. QE-18, pp.1669–1674, Oct. 1982.

[12] N. A. Olsson, H. Temkin, R. A. Logan, L. F. Johnson, G. J. Dolan, J.P. Van der Ziel, and J. C. Campbell, "Chirp-free transmission over 82.5km of single mode fibers at 2 Gbit/s with injection locked DFB semiconductor lasers," *IEEE J. Lightwave Technol.*, vol. LT-3, pp. 63–67, Feb.1985.

[13] X. Meng, T. Chau, and M. C.Wu, "Experimental demonstration of modulation bandwidth enhancement in distributed feedback lasers with external light injection," *Electron. Lett.*, vol. 34, no. 21, pp. 2031–2032, 1998.

[14] R. Olshansky,"", J. Lightwave Technology 7(1989) 1329

[15] S. Minin, M. R. Fisher, S. L. Chuang, "Current-controlled group delay using a semiconductor Fabry-Perot amplifier," *Applied Physics Letters*, vol. 84, pp. 3238-3240, 2004.

[16] X. Zhao, P. Palinginis, B. Pesala, C. J. Chang-Hasnain, P. Hemmer, "Tunable ultraslow light in vertical-cavity surface-emitting laser amplifier," *Optics Express*, vol. 13, pp. 7899-7904, 2005.

Chapter 2 High speed modulation of Quantum Dot VCSEL

In this chapter, we present monolithic quantum-dot vertical-cavity surface-emitting laser (QD VCSELs) operating in the 1.3 μm optical communication wavelength. The QD VCSELs have adapted fully doped structure on GaAs substrate. The output power is ~ 330 μW with slope efficiency of 0.18 W/A at room temperature. Single mode operation was obtained with side-mode suppression ratio of > 30 dB. Modulation bandwidth and eye diagram in 2.5 Gb/s was also presented.

2.1 Sample structure and Fabrication process

All structures were grown on GaAs (100) substrates by molecular beam epitaxy (MBE). The epitaxial structure was as follows (from bottom to top) - n+-GaAs buffer, 33.5-pair n+-$Al_{0.9}Ga_{0.1}As$/n+-GaAs (Si-doped) distributed Bragg reflector (DBR), undoped active region, p-$Al_{0.98}Ga_{0.02}As$ oxidation layer, 22-pair p+-$Al_{0.9}Ga_{0.1}As$/p+-GaAs DBR (carbon-doped) and p+-GaAs (carbon-doped) contact layer. The graded-index separate confinement heterostructure (GRINSCH) active region consisted mainly of three stack of QDs active region, with PL emission at 1.266 μm, embedded between two linear-graded $Al_xGa_{1-x}As$ (x = 0 to 0.9 and x = 0.9 to 0) confinement layers. The thickness of the cavity active region was 1λ. Carbon was used as the p-type dopant in the DBR to increase the carrier concentration (2-3×10^{18} cm-3). The interfaces of both the p-type and n-type $Al_{0.9}Ga_{0.1}As$/GaAs DBR layers are linearly graded to reduce the series resistance. The optical characteristics of QDs were optimized through PL measurement and structural analysis. The details of the process were fully described in our previous works [1]. The mesa diameter of the fabricated device is 26μm with a 5 μm oxide aperture, and the device surface is quasi-planar so that the annular p-contact metal and the bond pad are on the same level. The device structure is shown in Fig.2-1. The p-contact was formed by directly depositing Ti/Pt/Au on the upper heavily doped p$^+$ GaAs contact layer, and Au/Ge/Ni/Au was deposited on the bottom side of the substrate after it had been thinned down, and the shaded region beneath the bond pad represents the implanted region. It is worth noting that neither the intra-cavity /

co-planar metal contact nor polyimide resin planarization been used in the process. After metal annealing, the sample was immediately probe tested on the wafer level to extract the static operation characteristics, and was subsequently divided into two pieces. One piece was diced for packaging later, and the other was sent to be subjected to H^+ implantation with a dose of $10^{15} cm^{-2}$ for the purpose of further reducing the parasitic capacitance. Preliminarily we adopt four different proton energies in the range from 300 to 420keV according to the stopping and range of ions in matter (SRIM) simulation results, but the ideal combination of proton implantation energies in relative experiments currently we finished has not been optimized yet. The proton energy we used in this experiment was stronger than that used for conventional proton-implanted VCSELs. The reason for using such high-energy protons to bombard the sample is simply that the surface of the implanted region has already been passivated by the presence of 1500-Å-thick SiO_2 and 4000-Å-thick metal bond pad. When a charged particle such as H^+ penetrates a dielectric material such as SiO_2, it is subjected to scattering because of the built-in electric field result from the dipole and metal-insulator-semiconductor interfaces. However the incident proton has seldom been influenced by the thicker metal bond pad because there is no electric field inside the metal. Hence, we need a higher energy to make sure the implanted proton can penetrate the SiO_2 and eventually locate at the right depth, that is, as close as possible to the active region. The implantation region was kept apart the mesa to prevent the damage which was caused by ion bombardment from destroying the active region.

2.2 DC Characteristics of QD VCSEL

2.2.1 Experimental Setup

In order to precisely measure characteristics of QD VCSEL, such as LIV curve, optical spectrum, or near field pattern, we need to setup a system which can test our sample on wafer level or packaged level. Probe station was a basic instrument to meet our needs. Scheme of probe station system, illustrated in Figure 2-2, include probe station, current source, and power-meter module. Keithley 238 can provide precisely continuous current with laser diode and measure relative voltage synchronously. Newport power meter module (model 1835C) with photodiode and power meter can measure the light output power of the laser diode. An integration sphere was used to pick up whole emitting power from VCSEL to improve the accuracy of power measurement.

The VCSEL device was placed on a platform of the probe station and was injected bias current with microprobe. Threshold condition, slope efficiency, turn-on voltage and differential resistance can be obtained from L-I-V information by sweeping bias current. Near-field pattern was obtained by specific CCD. Emission spectrum of the device was measured by optical spectrum analyzer (OSA, Advantest 8381). A multi-mode fiber probe was placed close to the emission aperture to take optical spectra. The OSA had spectrum resolution of 0.1nm which was adequate to measure VCSEL lasing spectra.

2.2.2 Results and Discussion

Fig. 2-3 plots curves of light output and voltage versus current (LIV). The threshold current is ~ 1.8 mA and the threshold current density is 7.6 kA/cm^2. The output power rollover occurs as the current increases above 4mA with maximum optical output of 0.33mW at 20°C. In addition, the VCSEL is single polarization in the full operating range with ratio of ~20dB. Inset of Fig 2-3 is the near-filed pattern of the QD VCSEL biased at 3mA which indicated the fundamental mode lasing. Fig 2-4 shows the typical emission spectra of the quantum-dot VCSELs, which indicate single transverse mode operation in the whole operation range with a lasing wavelength of ~1.278 μm and side mode suppression ratio (SMSR) > 30dB.

To investigate the temperature dependence of the QD VCSEL, LI curves were measured from room temperature to 55°C with current step of 0.01 mA, as shown in Fig. 2-5. The threshold current varies only 0.15 mA (< 10% of I_{th}) with temperatures from 10°C to 45°C and the slope efficiency drops from 0.18 to 0.1 W/A. The small temperature dependence of threshold current corresponds to a characteristic temperature (T_0) of 450K, a high value comparing with the InGaAs(N) VCSEL in 1.3 μm. The high characteristic temperature was attributed to the wide gain spectra of the quantum dots gain media. When temperature increases, the wide gain spectra make the alignment between gain spectra and cavity resonance not sensitive, and therefore improve the T_0. However, increase of threshold current with temperature and the quench of output power were also observed after 50°C which implies the gain of the quantum dots decreases severely in higher temperature.

2.3 High speed modulation of QD VCSEL

2.3.1 Theory：Small signal modulation

Under small signal modulation, the carrier and photon density rate equation are used to calculate relaxation resonance frequency and its relationship to laser modulation bandwidth.

Consider the application of an above-threshold DC current, I_o, carried with a small AC current, I_m, to a diode laser. The small modulation signal with some possible harmonics of the drive frequency, ω. Small signal approximation, assumes $I_m << I_o$ bias and spontaneous emission term, β, is neglected, is expressed as

$$I = I_0 + I_m(t) = I_0 + I_m(w)e^{jwt}$$
$$n = n_0 + n_m(t) = n_0 + n_m(w)e^{jwt} \tag{2-1}$$
$$n_p = n_{p0} + n_{pm}(t) = n_{p0} + n_{pm}(w)e^{jwt}$$

Before applying these equations, the rate equation is rewritten for the gain. Assumption under DC current is sufficiently above threshold that the spontaneous emission can be neglected. Without loss of generality, we suppose full overlap between the active region and photon field, $\Gamma = 1$; furthermore, internal quantum efficiency, η_i, is neglected. That is,

$$\frac{dn}{dt} = \frac{I}{qV} - \frac{n}{\tau} - g_0(n - n_{tr})n_p \tag{2-2}$$

$$\frac{dn_p}{dt} = g_0(n - n_{tr})n_p + \beta R_{sp} - \frac{n_p}{\tau_p} \tag{2-3}$$

substitute Eq (2-1) into Eq(2-2) and Eq(2-3), it is similarly expressed modulation terms as

$$\frac{dn_m}{dt} = \frac{I_m}{qV} + g(n_0)n_{pm} - g_0 n_{p0} n_m - \frac{n_m}{\tau} \tag{2-4}$$

$$\frac{dn_{pm}}{dt} = g_0 n_{p0} n_m - g_0(n_0)n_{pm} - \frac{n_{pm}}{\tau_p} \tag{2-5}$$

The small signal terms in frequency domain of carrier and photon are given by

$$n_m(t) = n_m(w)e^{jwt}$$
$$n_{pm}(t) = n_{pm}(w)e^{jwt}$$

substitute into Eq(2-4) and (2-5), the equations become

$$jwn_m(w)e^{jwt} = \frac{I_m(w)e^{jwt}}{qV} + g(n_0)n_{pm}(w)e^{jwt} - g_0 n_{p0} n_m(w)e^{jwt} - \frac{n_m(w)e^{jwt}}{\tau}$$

Carrier modulation term in frequency domain is simplified as

$$jwn_m(w) = \frac{I_m(w)}{qV} + g(n_0)n_{pm}(w) - g_0 n_{p0} n_m(w) - \frac{n_m(w)}{\tau}$$

$$[jw - g_0 n_{p0} + \frac{1}{\tau}]n_m(w) = \frac{I_m(w)}{qV} + g(n_0)n_{pm}(w) \tag{2-6}$$

Photon modulation term in frequency domain is simplified as

$$jwn_{pm}(w) = g(n_0)n_{pm}(w) + g_0 n_{p0} n_m(w) - \frac{n_{pm}(w)}{\tau_p}$$

$$[jw - g(n_0) + \frac{1}{\tau_p}]n_{pm}(w) = g_0 n_{p0} n_m(w) \tag{2-7}$$

Solve for $n_m(w)$ and $n_{pm}(w)$ using Eq (2-6) and (2-7), we obtain the frequency response of two arranged equations as below

$$n_m(w) = (\frac{jw}{jw\Omega - w^2 - w_r^2})(\frac{I_m(w)}{qV}) \tag{2-8}$$

$$n_{pm}(w) = (\frac{\tau_p w_r^2}{jw\Omega - w^2 - w_r^2})(\frac{I_m(w)}{qV}) \tag{2-9}$$

where

$$w_r^2 = (2\pi f_r)^2 = (\frac{n_{p0}}{\tau_p})g_0 \tag{2-10}$$

$$\Omega = \frac{1}{\tau} + n_{p0} g_0 \tag{2-11}$$

With the Eq(2-8) and (2-9), we observe the coupling between the small signal photon, n_{pm}, and carrier, n_m. Small signal carrier injection induces photon achieved oscillation. This phenomenon produces a natural resonance in the laser cavity which shows up the output power of the laser in response to sudden changes in the input current. The natural frequency of oscillation associated with this mutual dependence between n_m and n_{pm}.

Modulation response is expanded the small signal modulation relationship to steady-state. From Eq.(2-8) and (2-9), the modulation response is denoted as

$$M(w) = \left| \frac{n_{pm}(w)}{n_{pm}(0)} \right| = \left| \frac{\dfrac{\tau_p w_r^2}{jw\Omega - w^2 - w_r^2}}{\dfrac{\tau_p w_r^2}{w_r^2}} \right| = \left| \frac{w_r^2}{jw\Omega - w^2 - w_r^2} \right| \tag{2-12}$$

Modulation bandwidth is determined as cutoff frequency, f_c, which is the position with half response written as

$$M(w_c) = \frac{1}{2} M(0) = \frac{1}{2} \frac{w_r^2}{[(w_c^2 - w_r^2)^2 + w_r^2 \Omega^2]} = \frac{1}{2} \tag{2-13}$$

for $w_r^2 \Omega^2 \ll (w_c^2 - w_r^2)^2$, the cutoff frequency, w_c, is approximated to $\sqrt{3} w_r$.

Transfer function, H(w), is the identical term in Eq(2-12). and respectively obtained with Cramer's rule. It is similar to modulation response, M(w), describing the response of the laser intensity to small variations in the drive current through the active region. That is,

$$H(f) = C \frac{f_r^2}{f_r^2 - f^2 + j\dfrac{f}{2\pi}\gamma} \tag{2-14}$$

where f_r is the resonance frequency same as Eq(2-10). γ is the damping rate similar to Eq.(2-11), and C is a constant. Accounting for additional extrinsic limitations due to carrier transport and parasitic elements related to the laser structure results in an extra pole in the small signal modulation transfer function

$$H(f) = C \left(\frac{f_r^2}{f_r^2 - f^2 + j\dfrac{f}{2\pi}\gamma} \right) \cdot \left(\frac{1}{1 + j\dfrac{f}{f_p}} \right) \tag{2-15}$$

where f_p is the cutoff frequency of the low pass filter characterizing the extrinsic limitations. It is crucial for microwave applications that the modulation bandwidth of the VCSEL is sufficiently large so that efficient modulation is achieved as the modulation frequency.

2.3.2 Experimental Setup：Microwave test system

The microwave test system was mainly consisted of network analyzer, Bias-Tee and high speed photodetector, as illustrated with Figure 2-6. Agilent 8720ES network analyzer was a crucial instrument of this microwave measurement. Transmitter of network analyzer produced -10dBm RF signal. Laser diode drivers (New port, model 525) provided direct bias current with the laser diode. Bias-Tee combined AC and DC signal transmission through the coaxial cable. The laser diode was hermetically sealed by a standard TO-Can laser package (TO-46) with a built-in lens. The laser diode TO-Can package and the single-mode fiber are assembled by laser welding technique, as shown in Figure 2-7. Then, we welded our device on a high speed SMA connector and connected with the coaxial cable. 25-GHz near-IR photodetector (New Focus, model 1414) was received the modulation light signal from the laser diode and was conversed into electrical signal and fed to network analyzer. Comparing two channels microwave signal by network analyzer, information of transmission and reflection characteristics could be expressed as vector(magnitude and phase), scalar(magnitude only), phase-only quantities, that was, S-parameter.

2.3.3 Results and Discussion

The small signal response of VCSELs as a function of bias current was measured at $25^{\circ}C$ using a calibrated vector network analyzer (Agilent 8720ES). Fig. 2-8 indicates the modulation frequency increases with the bias current low current range. At a bias current of larger than 2.5mA, the bandwidth saturate and the maximum 3dB modulation frequency response is measured as ~2 GHz. In Fig. 2-9, the 3dB bandwidth (f_{3dB}) is plotted as a function of the bias current. At low bias currents, the bandwidth increase in proportion to the square root of the current as expected from the rate equation analysis. The saturation of bandwidth was clearly observed as bias current increases above 2.5mA which might be attributed to heating effect. Carrier de-population in QDs subjected to the heated active region may suppress the material gain and put the intrinsic limit of high speed modulation. The modulation current efficiency factor (MCEF) is ~ 2.5 $GHz/(mA)^{1/2}$. Improvement can be done by increasing the quantum dots stacks and reducing the current density of each dot simultaneously. Finally, we illustrate the eye diagram at 1.25 Gb/s and 2.5 Gb/s, as shown in Fig 2-10. The QD VCSEL shows clear and symmetrical eye diagram at 1.25 Gb/s. At 2.5 Gb/s, the eye was degraded due to the overshoot and insufficient bandwidth. Future work will focus on enhancement of high speed performance by reducing the device parasitic and thermal impedance.

2.4 Conclusion

We present monolithic quantum-dot vertical-cavity surface-emitting laser (QD VCSELs) operating in the 1.3 μm optical communication wavelength. The QD VCSELs have adapted fully doped structure on GaAs substrate. The output power is ~ 330 μW with slope efficiency of 0.18 W/A at room temperature. Single mode operation was obtained with side-mode suppression ratio of > 30 dB. The high speed characteristics were also investigated. The free running bandwidth of QD VCSEL is ~2GHz. The modulation current efficiency factor (MCEF) is ~ 2.5 GHz/(mA)$^{1/2}$. Finally, we illustrate the eye diagram at 1.25 Gb/s and 2.5 Gb/s.

Reference

[1]H. C. Yu, S. J. Chang, Y. K. Su, C. P. Sung, Y. W. Lin, H. P. Yang, C. Y. Huang and J. M. Wang, "A simple method for fabrication of high speed vertical cavity surface emitting lasers," *Materials Science Engineering B,* vol. 106, pp. 101-104, 2004.
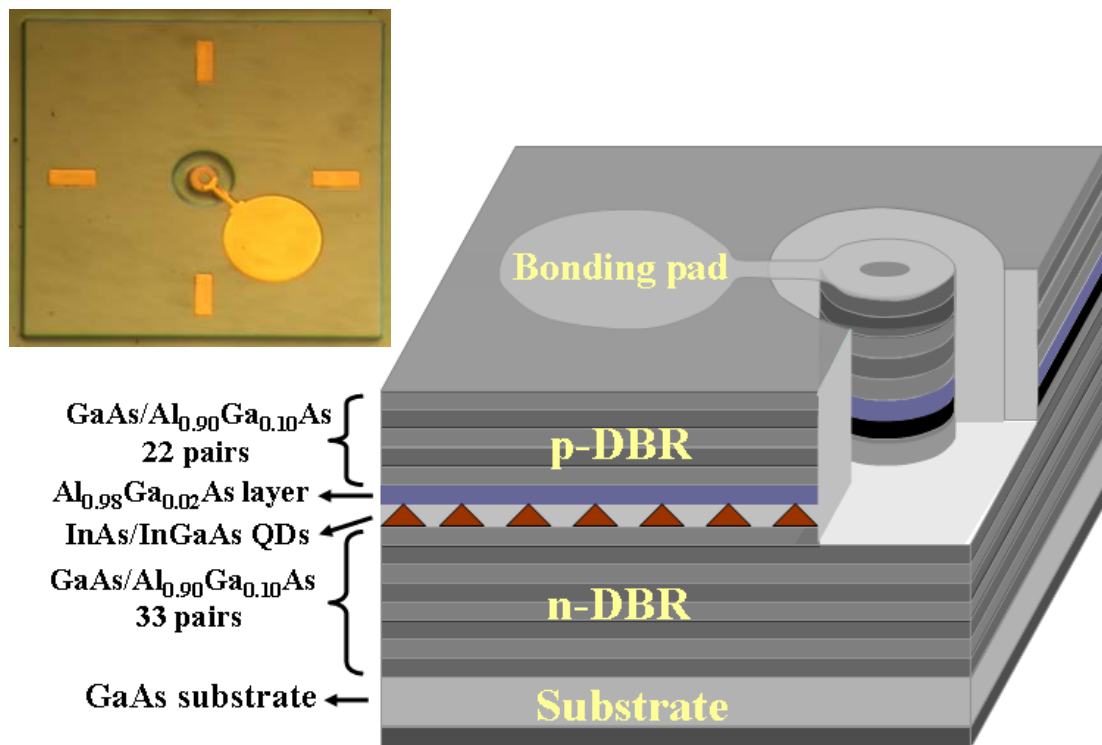
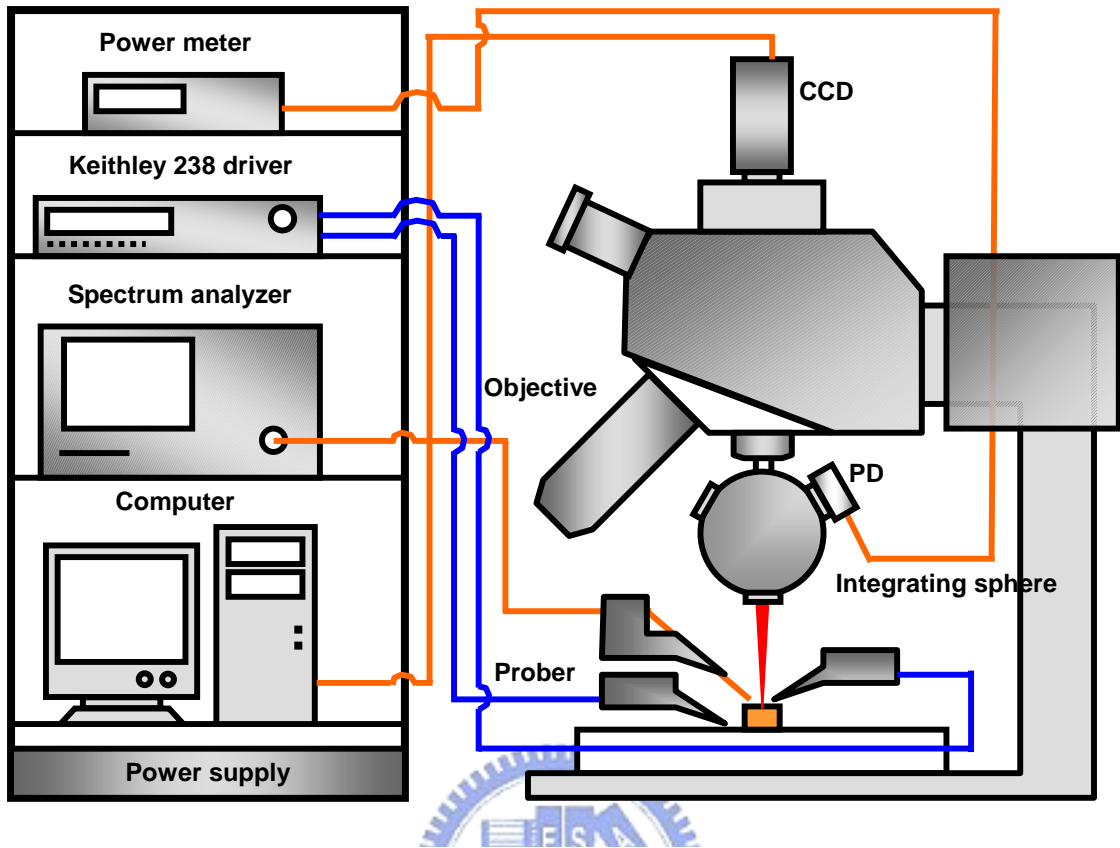**Fig. 2-1** QD VCSELs device structure. Inset is the top view image of the QD VCSEL.

Fig. 2-2 Probe station measurement instrument setup
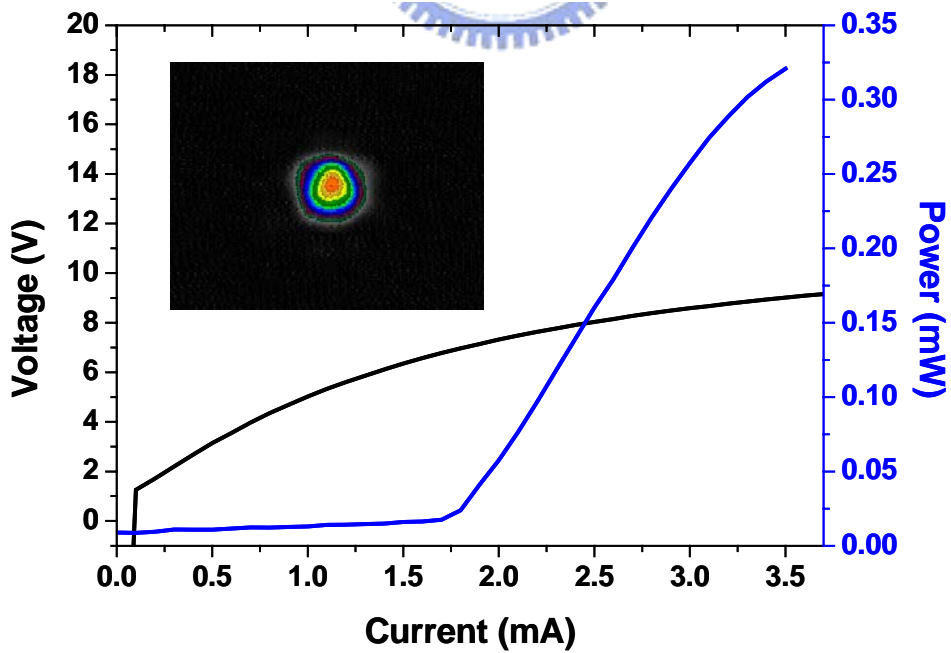
Fig. 2-3 L-I-V relationship of QD VCSEL. Inset is the near-filed pattern of the VCSELs at 3mA
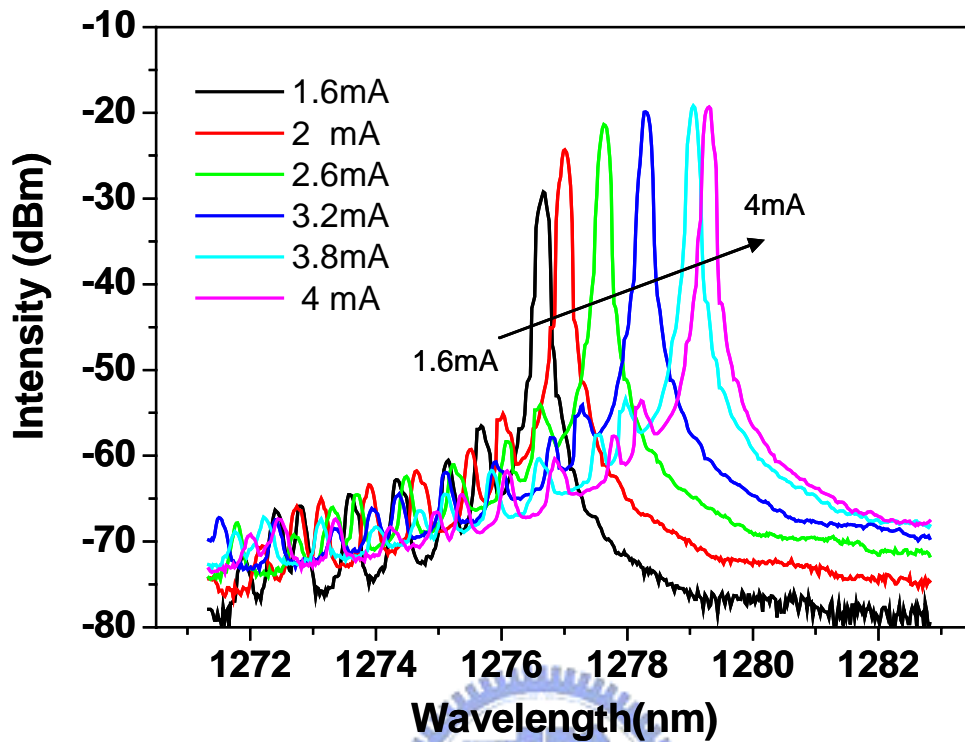
Fig. 2-4 Emission spectra of QD VCSEL at room temperature.
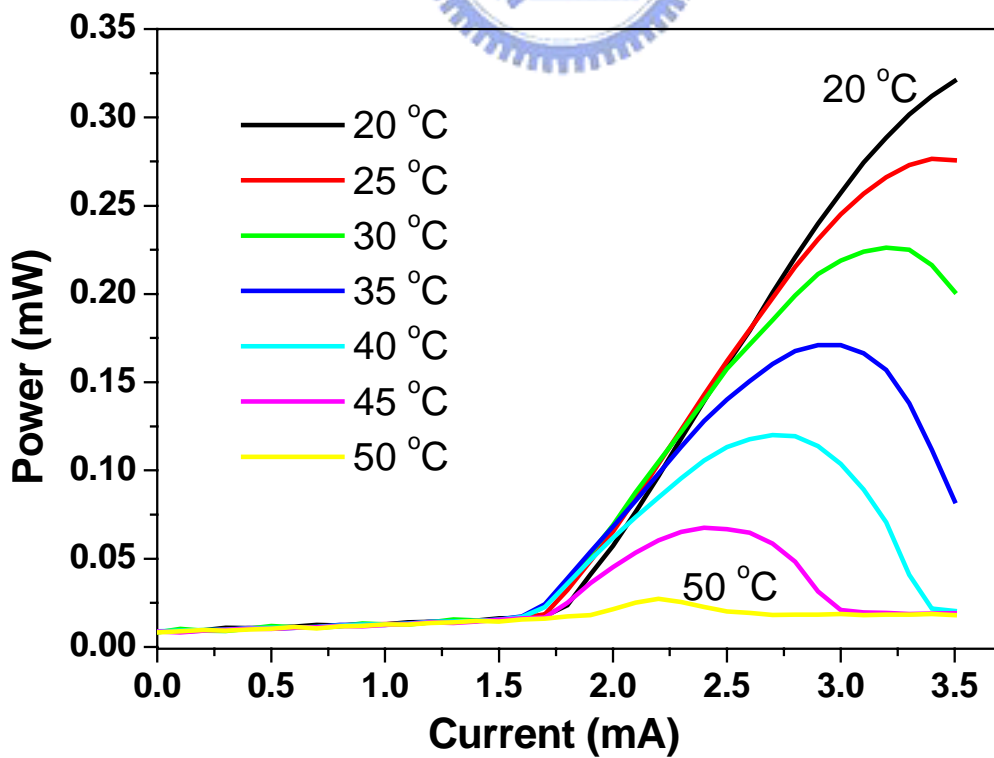
Fig. 2-5 Temperature dependent L-I relationship of QD VCSEL.

S11 : Reflection coefficient

S21: Frequency response
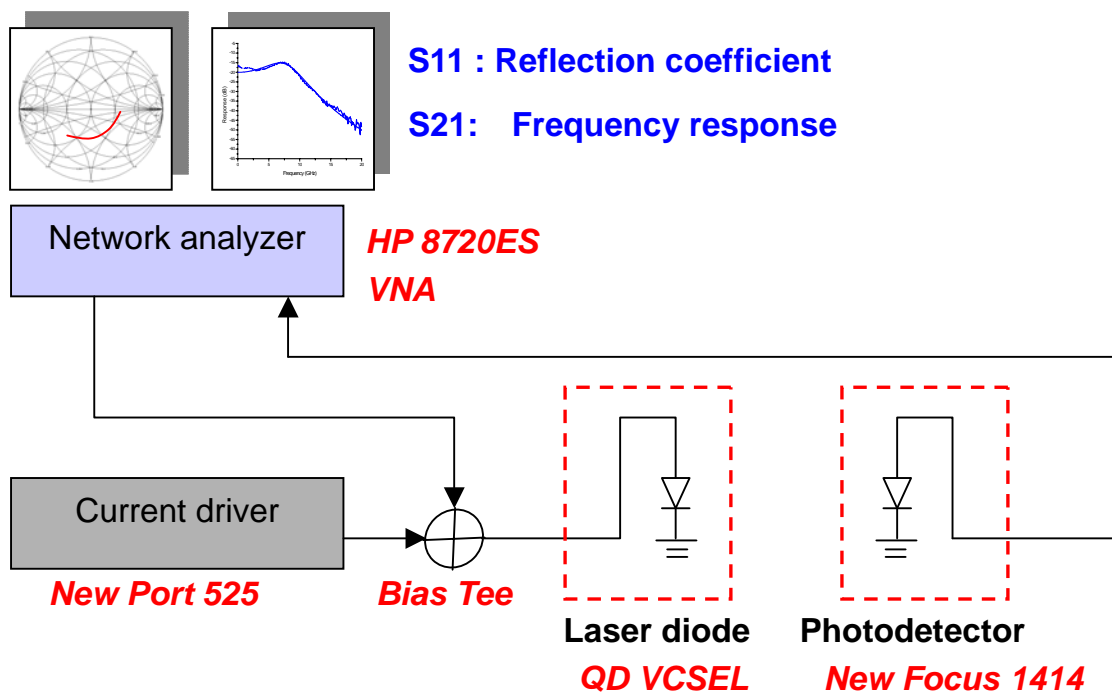
Fig. 2-6 Microwave test system setup

Fig. 2-7 The QD VCSEL TO-Can package and the single-mode fiber are assembled by laser welding technique.

Fig. 2-8 Small signal modulation response of QD VCSEL

Fig. 2-9 3dB frequency as a function of square root of current above threshold current.

(a)

(b)

Fig.2-10 Eye diagram of the QD VCSELs at (a) 1.25 Gb/s and (b) 2.5 Gb/s （ The time scale was 200 ps/div and 100 ps/div)

Chapter 3 Injection Locking of Quantum Dot VCSEL

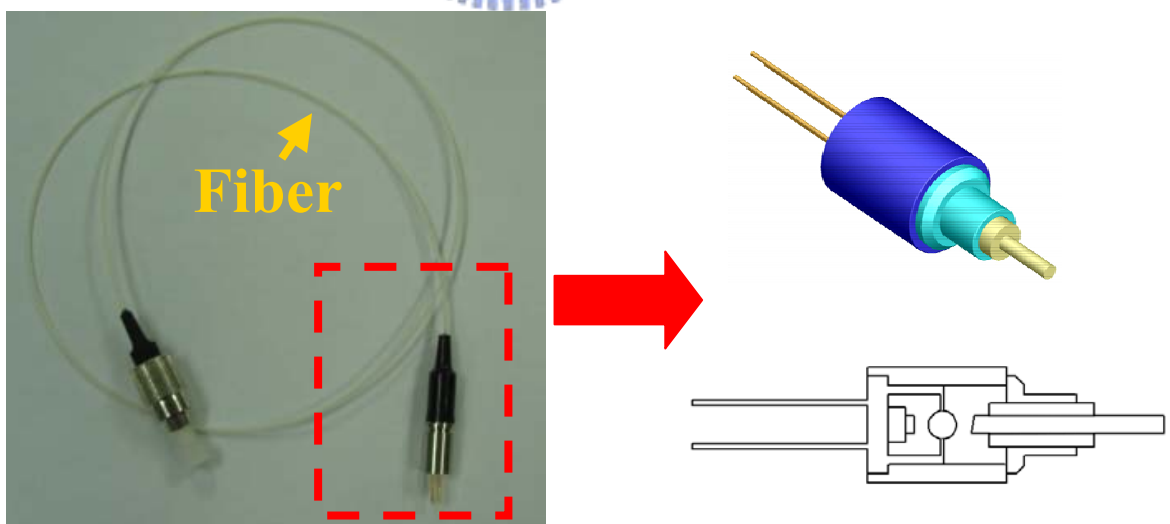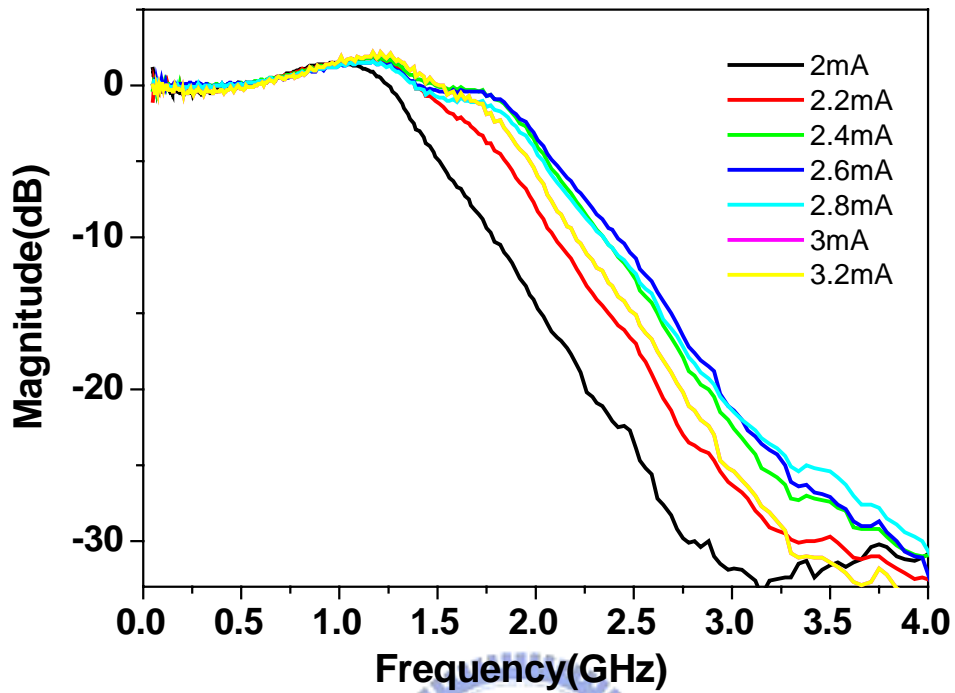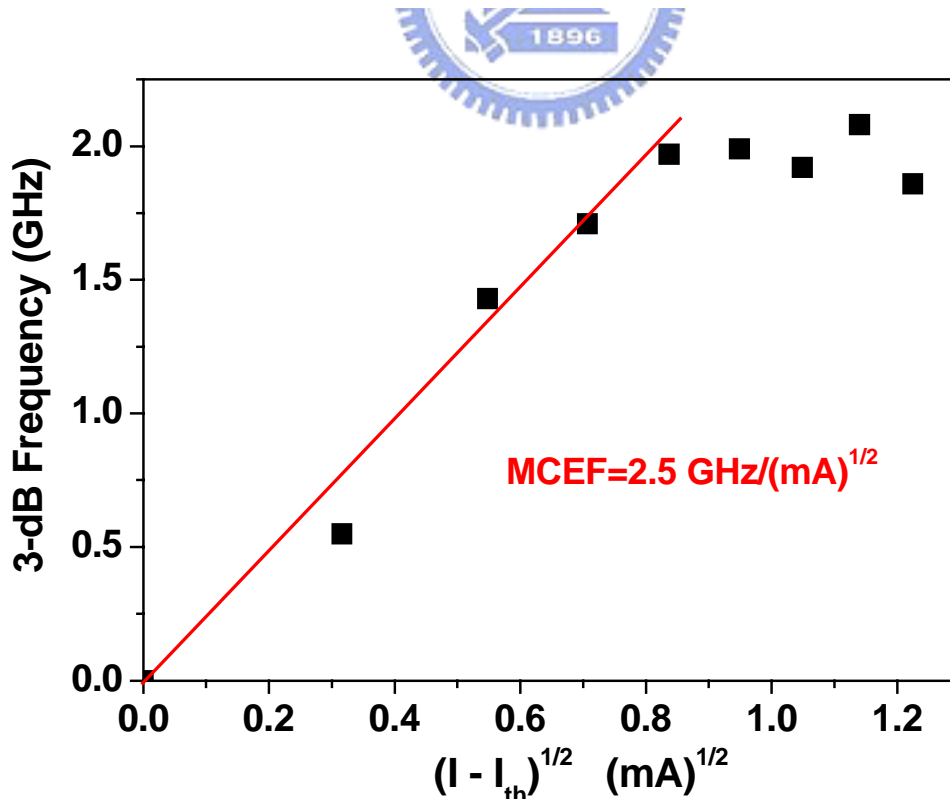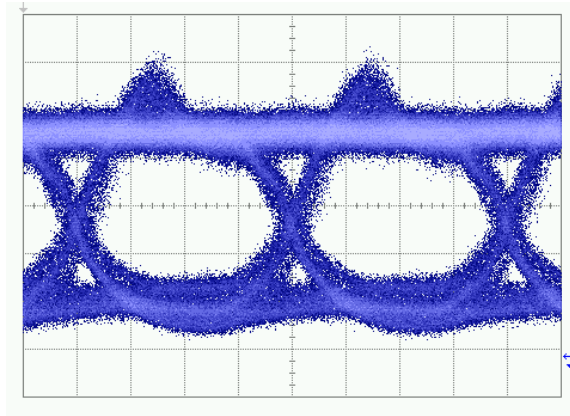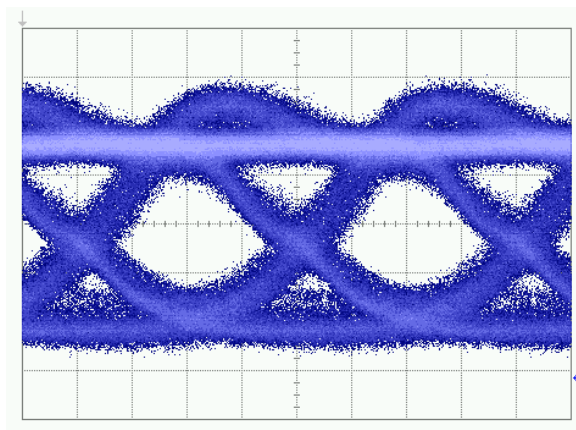This investigation experimentally demonstrates the dynamic characteristics of quantum dot vertical-cavity surface-emitting lasers (QD VCSEL) without and with light injection. The QD VCSEL is fully doped structure on GaAs substrate and operates in the 1.3 μm optical communication wavelength. The eye diagram, frequency response, and intermodulation distortion are presented. We also demonstrate that the frequency response enhancement by light injection technique allows us to improve the performance of subcarrier multiplexed system.

3.1 Modulation Response Enhancement by injection locking technique

3.1.1 Theory：Injection Locking Theorem

A rate equations based model is usually used to describe the interaction between photons and carriers inside a laser cavity. When an additional light source is injected into the cavity, the system preserves the general form of the original equations, but with extra terms describing the effects of the injection [1]. These extra terms play an important role in this nonlinear dynamic system and the equations are shown below.

$$\frac{dS}{dt} = [\frac{G_0(N-N_0)}{1+\varepsilon S} - \frac{1}{\tau_p}]S + 2k_c\sqrt{S \cdot S_{inj}} \cdot \cos(\Delta\phi(t)) + R_{sp} + F_s$$

$$\frac{d\phi}{dt} = \frac{\alpha}{2}G_0(N-N_{th}) - \Delta w + k_c\sqrt{\frac{S_{inj}}{S}} \cdot \sin(\Delta\phi(t)) + F_\phi \qquad (3\text{-}1)$$

$$\frac{dN}{dt} = \frac{I}{e} - \frac{N}{\tau_n} - \frac{G_0(N-N_0)}{1+\varepsilon S} \cdot S + F_n$$

In these equations, S, ϕ, and N denote the photon number, the phase, and the carrier number inside the follower laser cavity, respectively. G_0 denotes the gain coefficient, N_0 is the transparency carrier number, τ_p and τ_n are the photon and carrier lifetimes, respectively, I is the follower laser bias current, ε is the gain compression factor, and α is the linewidth-enhancement factor. R_{sp} is the spontaneous emission rate and the

Langevin noise terms F are also added for completeness. And $\Delta\phi(t)=\phi_{inj}-\phi(t)$ The follower laser locks to the master only for a certain combination of the injection power and frequency detuning. The stable locking condition can be found as [2]

$$-k_c\sqrt{\frac{S_{inj}}{S}}\sqrt{1+\alpha^2} < \Delta w < k_c\sqrt{\frac{S_{inj}}{S}}$$

rThe presence of the linewidth-enhancement factor makes the follower laser easier to lock to a master laser at the red side and, therefore, the locking range is asymmetric in frequency detuning. Also, a higher injection power results in a larger locking range. If the detuning range is mapped out for different injection powers, we obtain the locking range of the system.

We begin by assuming a steady-state value for each of the variables with a small signal modulation term, at the optical frequency

$$F_s = F_s(w)e^{jwt}, F_\phi = F_\phi(w)e^{jwt}, F_N = F_N(w)e^{jwt}$$
$$S = S_0 + S_1(w)e^{jwt}, \phi = \phi_0 + \phi_1(w)e^{jwt}, N = N_0 + N_1(w)e^{jwt}$$

(3-2)

Substituting (3.2) into (3.1),

Only considering the small- signal modulation terms in (3.2) for the photon part,

$$iwS_1(w) = \frac{G_0(N_0-N_{tr})}{1+\varepsilon S_0}S_1(w)(1-\frac{\varepsilon S_0}{1+\varepsilon S_0}) + \frac{G_0 N_1(w)}{1+\varepsilon S_0}S_0 - \frac{S_1(w)e^{iwt}}{\tau_p}$$
$$+ 2k_c(\sqrt{\frac{S_{inj}}{S_0}}\frac{S_1(w)}{2}\cos(\phi_0-\phi_{inj}) - \sqrt{S_0 S_{inj}}\sin(\phi_0-\phi_{inj})\phi_1(w)) + F_s(w)$$

(3-3)

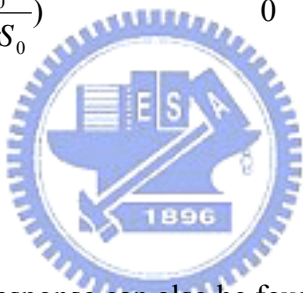Similarly, for the phase term, considering the small-signal modulation terms in (3.2),

$$iw\phi_1(w) = \frac{\alpha G_0 N_1(w)}{2} - k_c(\sqrt{\frac{S_{inj}}{S_0}}(-\frac{S_1(w)}{2}\sin(\phi_0-\phi_{inj}) + \cos(\phi_0-\phi_{inj})\phi_1(w)) + F_\phi(w)$$

(3-4)

Finally, for the carrier term,

$$iwN_1(w) = -\frac{N_1(w)e^{iwt}}{\tau_s} - \frac{G_0(N_0 - N_{tr})}{1 + \varepsilon S_0}S_1(w)(1 - \frac{\varepsilon S_0}{1 + \varepsilon S_0}) - \frac{G_0 N_1(w)}{1 + \varepsilon S_0}S_0 + F_n(w) \quad (3\text{-}5)$$

Equations (3.3), (3.4), (3.5) can now be written in matrix form:

$$A \begin{bmatrix} S_1 \\ \phi_1 \\ N_1 \end{bmatrix} = \begin{bmatrix} F_s \\ F_\phi \\ F_N \end{bmatrix}$$

$$A = \begin{bmatrix} iw - \dfrac{G_0(N_0 - N_{tr})}{1 + \varepsilon S_0}(1 - \dfrac{\varepsilon S_0}{1 + \varepsilon S_0}) \\ + \dfrac{1}{\tau_p} - k_c \sqrt{\dfrac{S_{inj}}{S_0}}\cos(\phi_0 - \phi_{inj}) & 2k_c\sqrt{S_0 S_{inj}}\sin(\phi_0 - \phi_{inj}) & -\dfrac{G_0}{1 + \varepsilon S_0}S_0 \\[2em] -\dfrac{k_c}{2}\sqrt{\dfrac{S_{inj}}{S_0{}^3}}\sin(\phi_0 - \phi_{inj}) & iw + k_c\sqrt{\dfrac{S_{inj}}{S_0}}\cos(\phi_0 - \phi_{inj}) & -\dfrac{\alpha}{2}G_0 \\[2em] \dfrac{G_0(N_0 - N_{tr})}{1 + \varepsilon S_0}(1 - \dfrac{\varepsilon S_0}{1 + \varepsilon S_0}) & 0 & iw + \dfrac{G_0}{1 + \varepsilon S_0}S_0 + \dfrac{1}{\tau_s} \end{bmatrix}$$

The small-signal modulation response can also be found from this system by considering I as the small signal modulation current.

$$\begin{bmatrix} S_1 \\ \phi_1 \\ N_1 \end{bmatrix} = A^{-1}\begin{bmatrix} 0 \\ 0 \\ I \end{bmatrix}$$

The modulation response transfer function will be

$$H(w) = \frac{|S_1(w)|}{I(w)}$$

Based on the above analysis, the small signal modulation response of the injection locked laser has been shown to be of the same form as that of a free-running laser with an additional 1st order pole :

$$H(s) \propto \frac{s + a_0}{s^3 + b_2 s^2 + b_1 s + b_0} \propto \frac{1}{1 + jwK} \cdot \frac{1}{w_R{}^2 - w^2 + jw\gamma} \quad (3\text{-}6)$$

In this equation, $s = jw$ and K represents he 1st order pole introduced by the injection, w_R the resonance and the damping term. The coefficients a_i and b_i are functions of the laser parameters and injection conditions [3].

The frequency response of this system is simplified considerably when $S_{inj}=0$ (i.e. no injected light). In this case, $a_0=b_0=0$, and the frequency response in equation (3-6) is reduced to $H(w) = A \dfrac{1}{(jw)^2 + b_2(jw) + b_1}$. This is the familiar two-pole equation for a directly modulated laser and the relaxation oscillation frequency is

$$f_r = (2\pi)^{-1}\sqrt{b_1} \sim (2\pi)^{-1}\sqrt{a_N S/\tau_P}$$

On the other hand, when S_{inj}/S is very large, b_0 becomes negligible compared to the other terms in the denominator of the transfer function, which is once again reduced to a two-pole function, $H(w) = A \dfrac{jw + a_0}{[(jw)^2 + b_2(jw) + b_1](jw)}$. with now

$b_1 \approx -k_c^2 \dfrac{S_{inj}}{S}$ and $f_r = \dfrac{\sqrt{|b_1|}}{2\pi}$. This is very interesting as it seems to indicate that

with strong injection fr can be increased indefinitely.

3.1.2 Experimental Setup：Injection Locking System

The experimental setup is schematically illustrated in Fig.3-1. The QD VCSEL is used as the slave laser while a DFB laser is used as the master laser. The injection power is varied by a variable optical attenuator at the output of the DFB laser. The polarization of the DFB laser is adjusted using a polarization controller before injecting into the QD VCSEL. The adjusted DFB laser signal injects into the port 1 of optical circulator then injecting into QD VCSEL at the port 2. The QD VCSEL is directed modulated by vector network analyzer. The light output at port 3 of optical circulator is divided into 2 parts. 90% of the light signal is transmitted into photo detector then convert into electrical signal amplified by RF amplifier and sent into vector network analyzer to measure frequency response. 10% of the light signal is connected to optical spectrum analyzer to observe the locking condition. In the experiment, the polarization and the center wavelength of DFB laser are adjusted that the QD VCSEL has the most significant enhancement in the frequency response. The wavelength detuning is adjusted by changing the temperature and bias current of DFB laser.

3.1.3 Results and Discussion

The free running frequency response of the QD VCSEL is shown as Fig.3-2 and the inset of Fig.3-2 shows the spectra of QD VCSEL. Fig. 3-3 shows the frequency response of the QD VCSEL with light injection and the QD VCSEL is biased at 4 mA. The detuning wavelength (λ_{DFB}- $\lambda_{QD\ VCSEL}$) is 0.128nm. This figure clearly shows that external light injection can achieve a significant enhancement in frequency response. When the power injection is 6dBm, the 3-dB frequency is from 1.75GHz to 7.44GHz which is the most improved bandwidth. The inset of Fig.3-3 is the spectra of QD VCSEL with and without light injection. After injection locking, the wavelength of QD VCSEL is red shift due to the injection wavelength of DFB laser longer than

QD VCSEL and the power level of QD VCSEL light output is enhanced by external light injection. We plot the 3dB frequency verses injection power as shown in Fig. 3-4. In this figure, we can observe that the 3dB frequency is enhanced by injection power of DFB laser. This is because external light injection in the active region of QD VCSEL makes the photon number increase thus improving the 3dB bandwidth. To prove the improved bandwidth can be utilized, we also demonstrated that this enhancement of the frequency response can greatly improve the performance of SCM system based on direct modulation of QD VCSELs.

. Fig. 3-5 shows the experimental setup for the injection locking of QD VCSEL in a SCM system. A 50 Mb/s non-return-to-zero (NRZ) pseudo-random binary sequence (PRBS) data with $2^{31} - 1$ pattern length from a pattern generator is mixed with a 7 GHz RF carrier. The resulting data signal is then used to directly modulate the QD VCSEL. Fig.3-6 shows the electrical spectra of QD VCSEL with and without light injection at point A. Light injection technique leads to 33 dB improvement in the SCM system. The 7-GHz 50-Mb/s is down converted using a mixer, where it is mixed with the same RF carrier generated by the signal generator. The variable phase shifter is used to adjust the carrier's phase. The corresponding eye diagrams are shown in Fig. 3-7. The improvement in system performance can be clearly seen when light injection technique is employed. The QD VCSEL without light injection cannot generate 7-GHz 50-Mb/s data due to the limited frequency response.

3.2 Reduction of nonlinear distortion by injection locking technique

We also study the reduction of nonlinear distortion in the QD VCSEL by light injection technique. Nonlinear distortion of the laser is important consideration for SCM systems. It can be characterized by measuring third-order intermodulation distortion (IMD3). The IMD3 is caused by two closely subcarrier frequencies. For

SCM systems, the IMD3 has the largest impact on performance degradation because of the IMD3 signal close to the original subcarrier frequencies [4].

3.2.1 Theory

The goal of any transmission system is to transfer information as accurately as possible. However, neither device is perfectly linear, particularly when large modulation levels are involved. Several different types of distortion products are common from these components such as harmonic distortion and intermodulation distortion.

When laser is intensity modulated there will be modulated signal power at he modulating frequency; and depending on the linearity of the device, there will also be some modulating power at harmonics of the modulating frequency. Some modulated power at the second harmonic and third harmonic of the modulating frequency is very common. Harmonic distortion is defined as the ratio of modulated power in harmonic of the modulating frequency to the power at the modulating frequency. For example:

$$HD_2 = \frac{P(2f_{mod})}{P(f_{mod})}$$

$$HD_3 = \frac{P(3f_{mod})}{P(f_{mod})}$$

$$THD = \frac{P(2f_{mod}) + P(3f_{mod}) + ... + P(nf_{mod})}{P(f_{mod})}$$

where HD_2 is the second harmonic distortion, HD_3 is the third harmonic distortion, and THD is the total harmonic distortion[5].

It is common to express the distortion in decibels (dB). In this case, the harmonic distortion is expressed as:

$$HD_x = 10\log(\frac{P(xf_{mod})}{P(f_{mod})})$$

Intermodulation distortion (ID) occurs when two or more modulating signals are present. In this case, device nonlinearities cause the two modulating signals to interact, producing new signals at the sum and difference frequencies. Second-order

intermodulation distortion for two signals can e measured as:

$$ID_2(f_i \pm f_j) = \frac{P(f_i \pm f_j)}{P(f_i)}$$

where $P(f_i) = P(f_j)$.

A particularly distressing form of intermodulation distortion is third-order intermodulation (IMD) for two closely spaced signals. This is because the IMD signals fall close to the original modulating frequencies.

$$IMD(2f_i - f_j) = \frac{P(2f_i - f_j)}{P(f_i)}$$

3.2.2 Experimental Setup

Fig. 3-8 shows the experimental setup for measuring the IMD3 of QD VCSEL with and without light injection. A commercial DFB laser is used as the master laser in our experiments. The injection power is controlled by a variable optical attenuator at the output of the DFB laser. The polarization of the DFB laser is adjusted using a polarization controller. The polarization is chosen that the second harmonic distortion of QD VCSEL has the must reduction. An optical circulator is used to couple the DFB laser light into the QD VCSEL. The QD VCSEL is modulated as single tone or two tone measurements by RF signal generator.

3.2.3 Results and Discussion

Fig. 3-9 (a) shows the electrical spectrum of the QD VCSEL without light injection under a 1 GHz microwave modulation. The microwave power level before the bias-T is 3 dBm. The second harmonic distortion of the QD VCSEL without light injection is -8.2 dB. Fig. 3-10 (b) shows the corresponding spectrum of the QD VCSEL with light injection. The central wavelength of DFB laser is 1277.99 nm, and the injection power is 2 dBm. The second harmonic distortion has been dramatically reduced to -26.4 dB. Fig. 3-10 (c) shows the measured second harmonic distortion as a function of the modulation frequency for QD VCSEL with and without light injection. Compared with the QD VCSEL without light injection, the second harmonic

distortion of QD VCSEL with light injection has been suppressed by more than 14 dB from 100 MHz to 1.2 GHz.

Two-tone measurements without and with light injection varied with the input RF power is also investigated, as shown in Fig. 3-10. The two-tone frequencies are 1 and 1.01 GHz. The fundamental tone power increase of 4.5dB and the distortion suppression of 10.6 dB are observed. As a result, the dynamic range of the QD VCSEL with light injection can be enhanced 15.1 dB for the IMD3.

3.3 Conclusion

In this chapter, we report the dynamic characteristics of QD VCSEL without and with external light injection. The significant enhancement of frequency response by light injection technique has been studied. The 3 dB frequency response has been increased by as much as 4.2 times using light injection technique. Moreover, this frequency response enhancement can improve the performance of SCM system. Experimental results show a 33 dB improvement in system performance. Furthermore, reduction of IMD3 in the QD VCSEL also has been observed. The dynamic range of the QD VCSEL with light injection can be enhanced 15.1 dB for the IMD3.These results show that external light injection is a very powerful technique to upgrade QD semiconductor lasers.

Reference

[1] N. Schunk and K. Petermann, "Noise analysis of injection-locked semiconductor injection lasers," *IEEE Journal of Quantum Electronics*, vol. QE-22, pp. 642-50,1986.

[2] C. H. Henry, N. A. Olsson, and N. K. Dutta, "Locking range and stability of injection locked 1.54-_m InGaAsP semiconductor lasers," *IEEE J. Quantum Electron.*, vol. QE-21, pp. 1152–1156, Aug. 1985.

[3] Lukas Chrostowski, Optical Injection Locking of Vertical Cavity Surface Emitting Lasers (A dissertation for the degree of Doctor of Philosophy, 2003).

[4] W. I. Way, Broadband Hybrid Fiber/Coax Access System Technologies (Academic Press, San Diego, 1999).

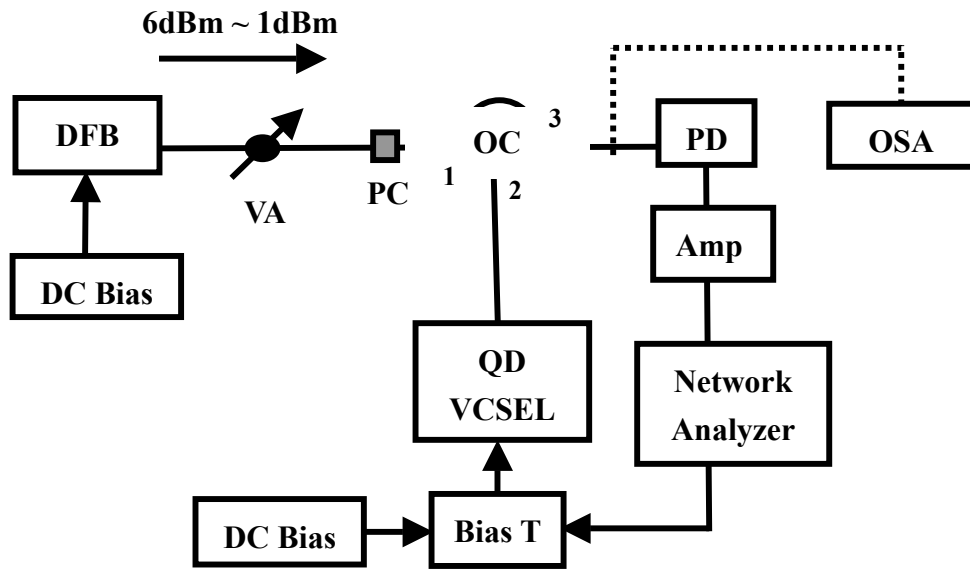[5] Dennis Derickson, Fiber Optic Test and Measurement (Prentice-Hall, Inc. 1998)

Fig. 3-1 (a) Schematic diagram of the quantum dot vertical cavity surface emitting laser (b) Experimental setup for the injection locking of QD VCSEL (DFB: DFB laser, VA: variable optical attenuator, OC: optical circulator, OSA: optical spectrum analyzer, PC: polarization controller, PD: photodetector, Amp: electrical amplifier)
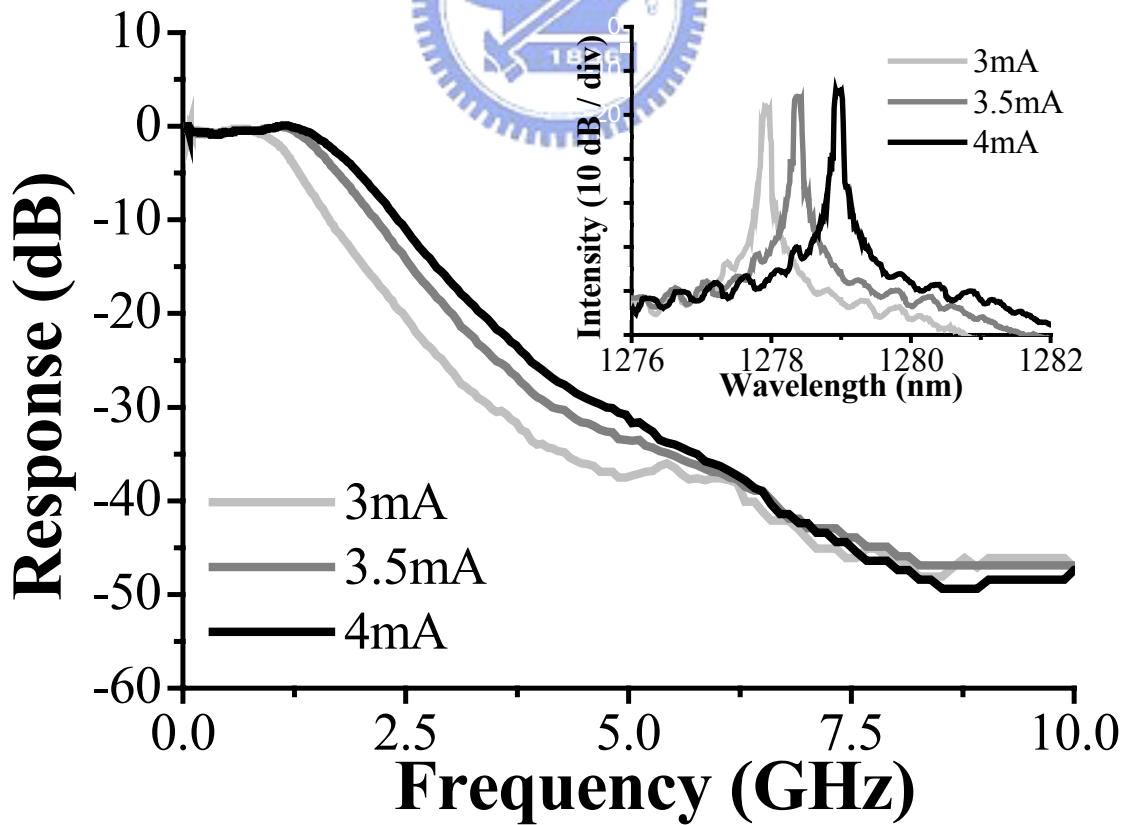

Fig. 3-2 Small-signal frequency response of QD VCSEL at different bias currents.
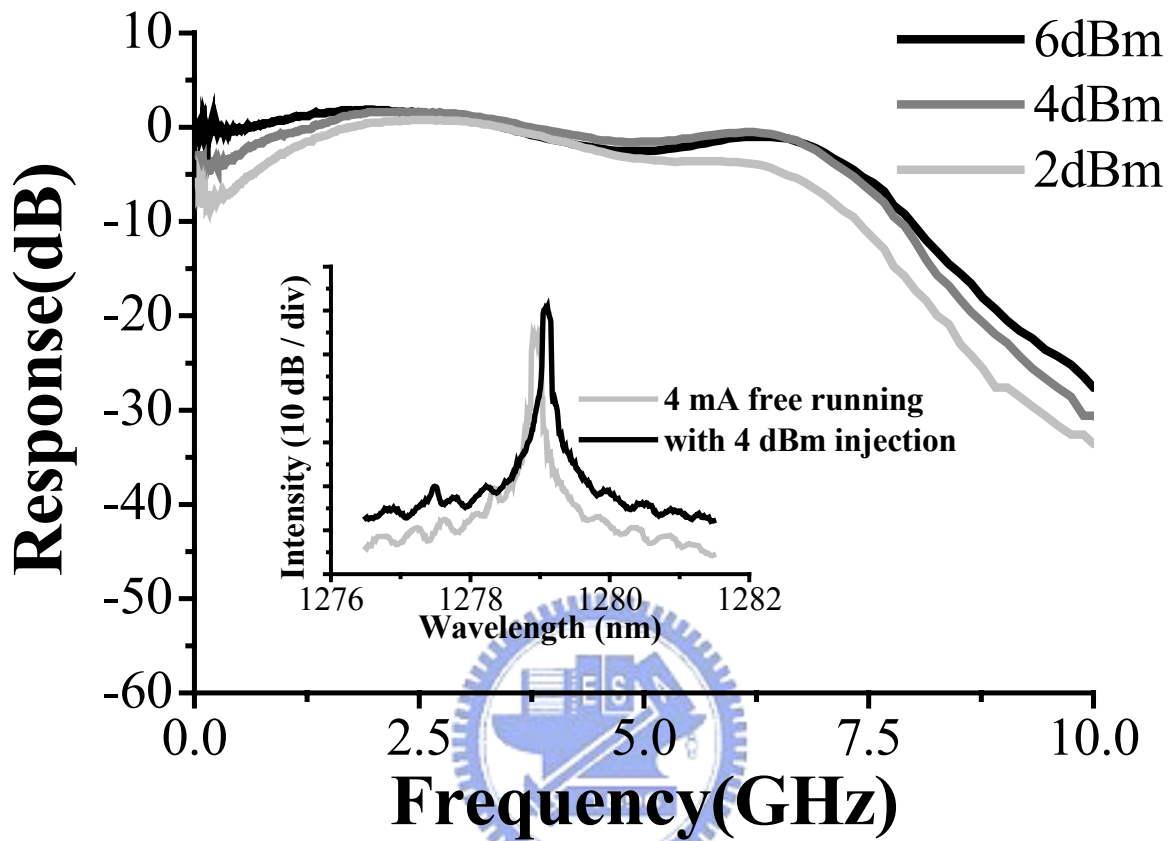
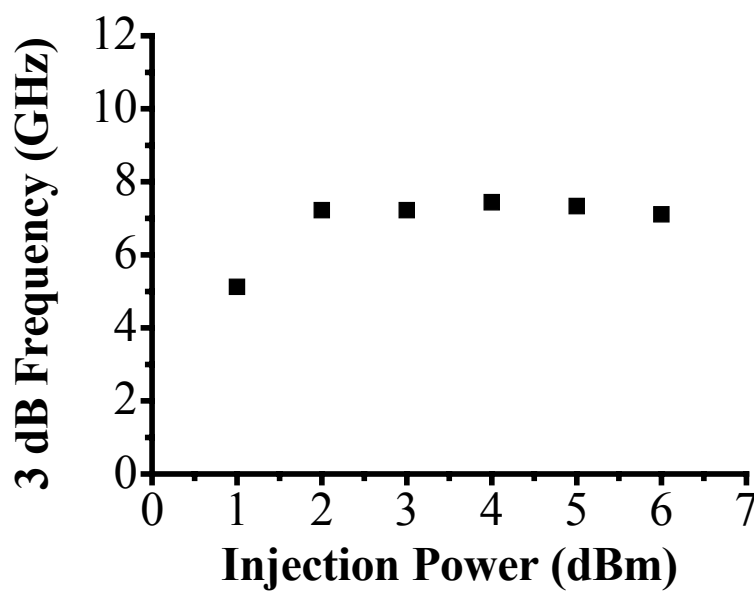**Fig. 3-3** Small-signal frequency response of QD VCSEL at different injection powers.

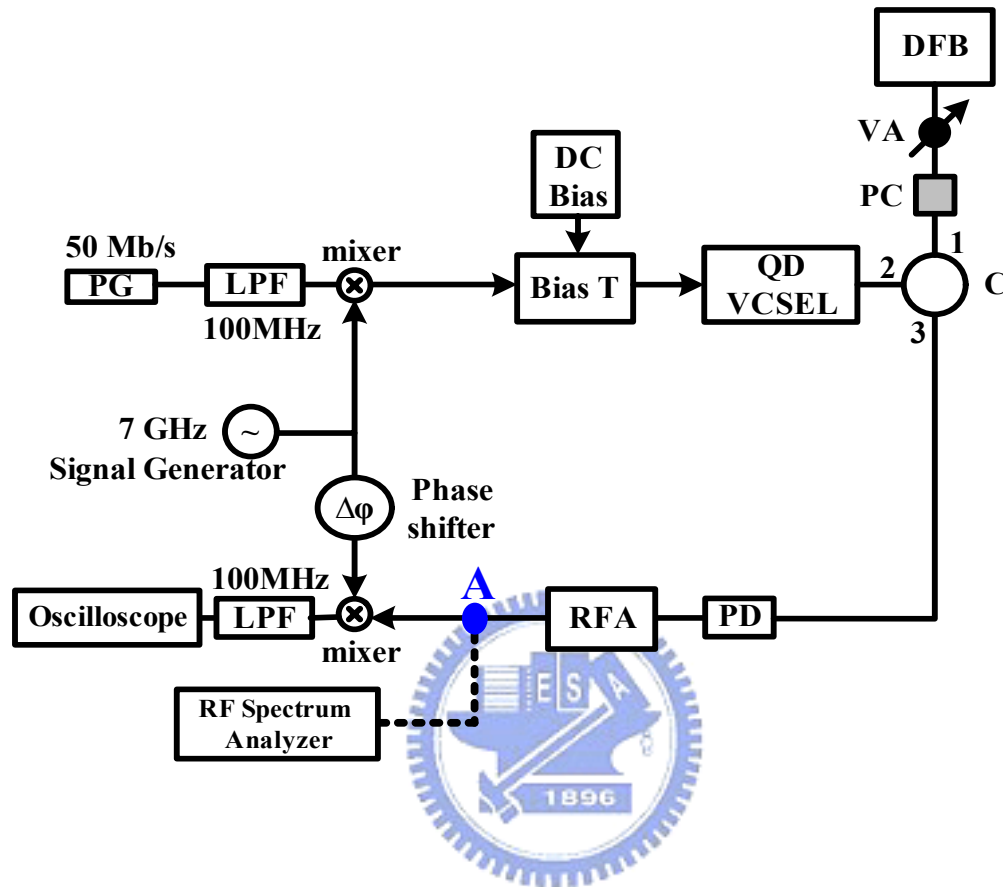**Fig. 3-4** 3 dB frequency response as a function of injection power.

Fig. 3-5 Experimental setup for the quantum dot VCSEL without and with light injection in a subcarrier multiplexed system. (PG: pattern generator, LPF: low pass filter, RFA: RF amplifier, PD: photodetector)

Intensity (5 dB / div)

(a) without light injection

(b) with light injection

6.90   6.95   7.00   7.05   7.10
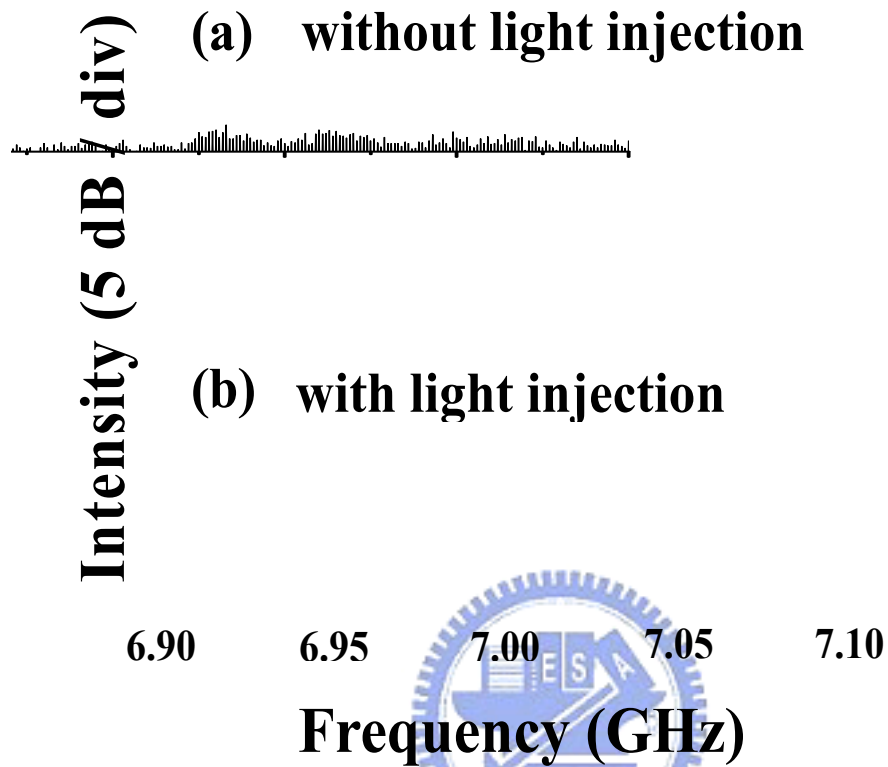
Frequency (GHz)

Fig. 3-6 7-GHz 50-Mb/s data signal at point A (a) without light injection (b) with light injection.
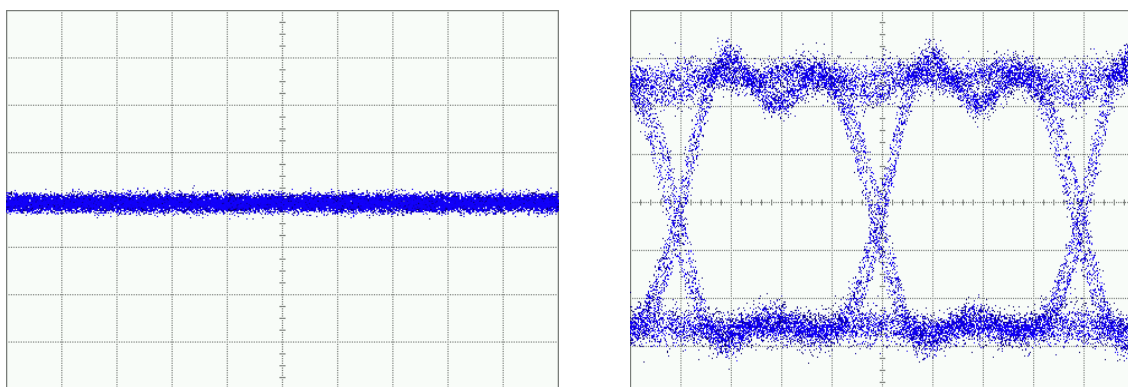

Fig. 3-7 Received eye diagrams of 50-Mb/s signal.

Fig. 3-8 Experimental setup for measuring the third-order
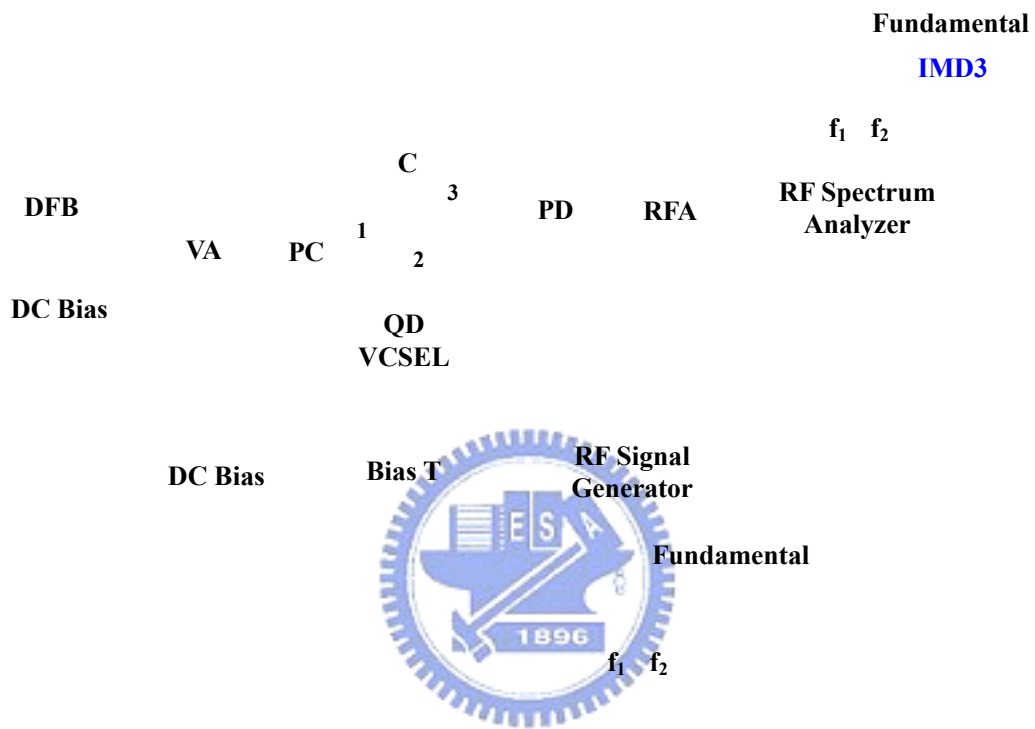intermodulation distortion (IMD3) of quantum dot
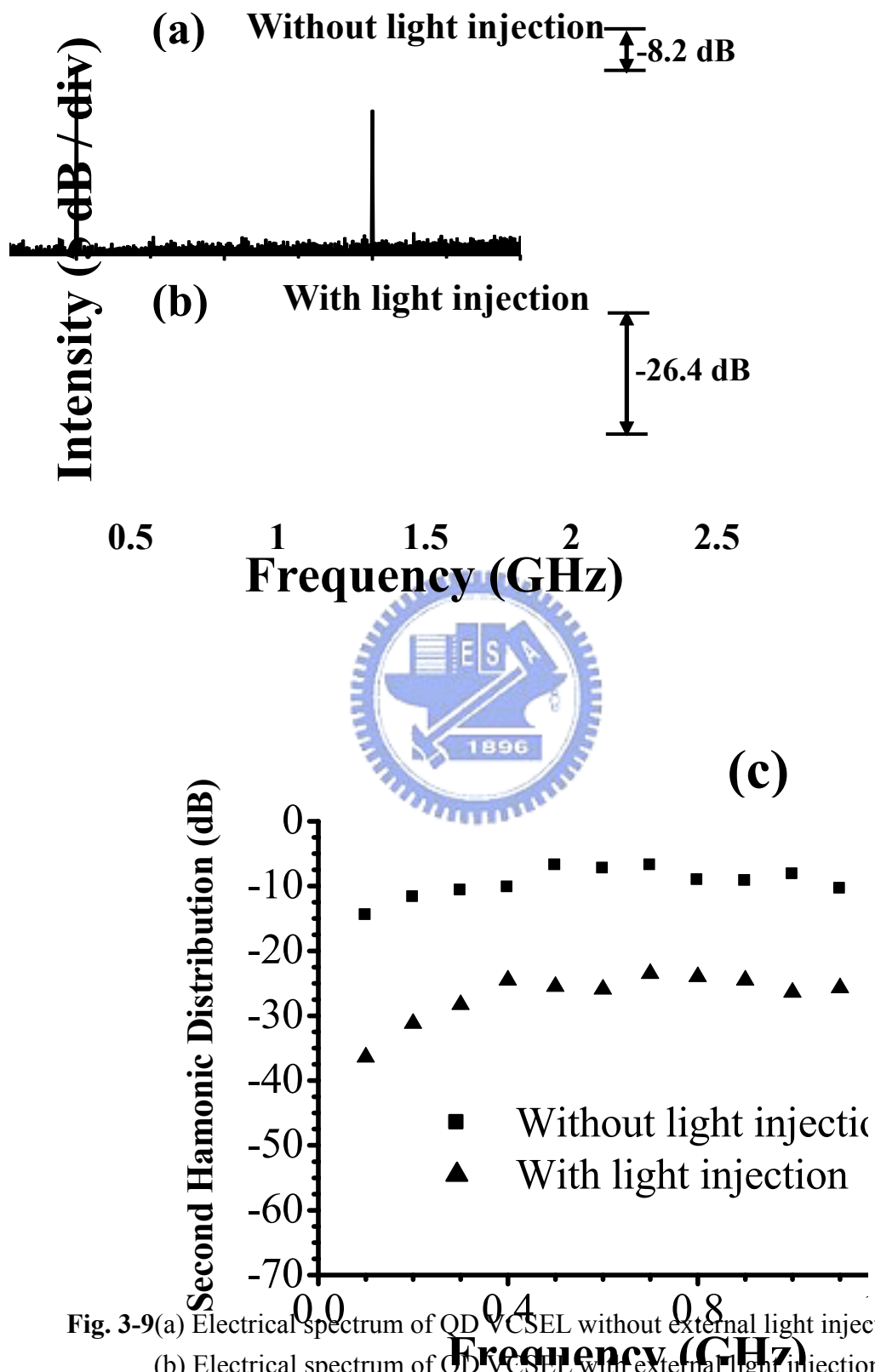VCSEL without and with light injection.

Fig. 3-9(a) Electrical spectrum of QD VCSEL without external light injection

(b) Electrical spectrum of QD VCSEL with external light injection

(c) Second harmonic distortion as a function of modulation frequency

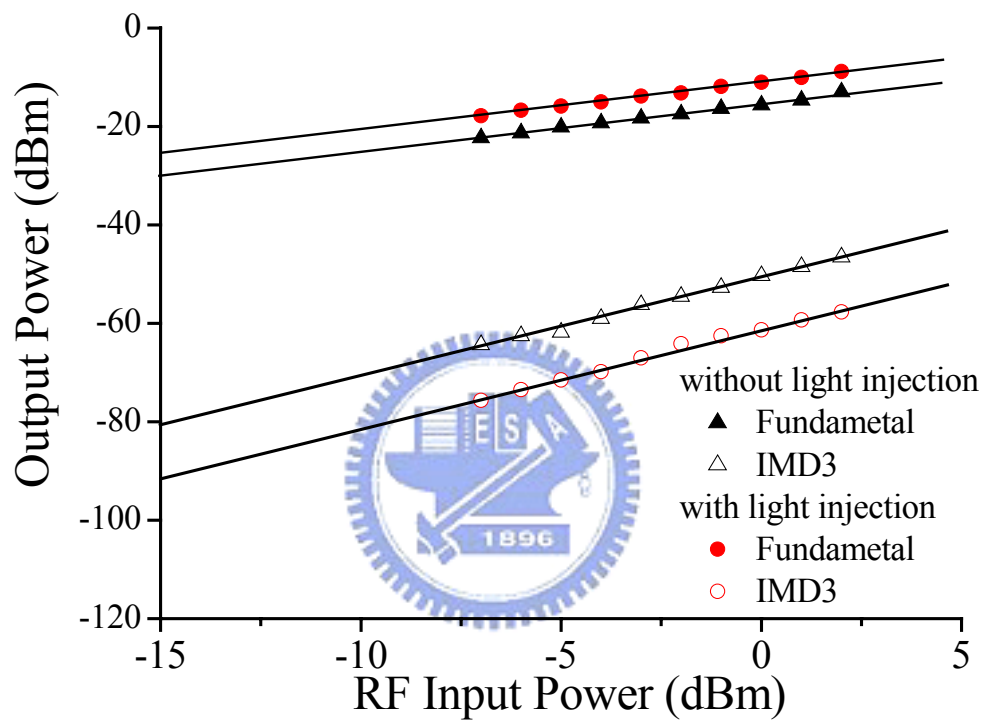for the QD VCSEL with and without external light injection.

Fig. 3-10 IMD3 of quantum dot VCSEL without and with light injection.

Chapter 4 Slow Light in Quantum Dot VCSEL

This investigation experimentally demonstrates tunable slow light in a 1.3 μm quantum dot vertical-cavity surface-emitting laser (QD VCSEL) at 10 GHz. The QD VCSEL fabricated on a GaAs substrate is grown by molecular beam epitaxy with fully doped n- and p-doped AlGaAs distributed Bragg reflectors. Tunable optical group delays are achieved by varying the bias currents, and the maximum delay of 42 ps at 10 GHz has been demonstrated at room temperature. Moreover, the delay-bandwidth product is 0.42.

4.1 Theory: Approaches to achieve slow light

To obtain a slow light device, in general, one must vary the medium within which the optical signal travels by either increasing the path length or reducing the signal group velocity. The former can be accomplished with the use of a fiber delay line, which will be discussed below. The latter has several possibilities. We first observe that the group velocity is defined as

$$v_g = \frac{\partial w}{\partial k} = \frac{c - w\dfrac{\partial n}{\partial k}}{n + w\dfrac{\partial n}{\partial w}} \tag{4-1}$$

where n is real part of the refractive index and k is the waveguide propagation constant. We can define a slowdown factor S as

$$S = \frac{c}{v_g} = \frac{n + w\dfrac{\partial n}{\partial w}}{1 - \dfrac{w}{c}\dfrac{\partial n}{\partial k}} \tag{4-2}$$

From (4-2), we see that the group velocity can be reduced by introducing a large and positive waveguide dispersion $\dfrac{\partial n}{\partial k}$ or material dispersion $\dfrac{\partial n}{\partial w}$. The waveguide dispersion can be designed using gratings or periodic structure [1]. However, the most effective method is to introduce a large material dispersion using EIT. Of course, it is

also possible to include both material and waveguide dispersion in one device to have an enhanced effect [2].

a. Optical Fiber Delay Lines:

Optical fiber delay lines have previously been referred to as an "optical buffer" [3]. One basic design typically consists of a 2×2 optical switch connected with a fiber loop. Other components such as optical isolators, amplifiers, and dispersion compensation devices have also been included to reduce impairments due to reflection, loss, and dispersion.

The optical switch is first set to direct the data train into the fiber loop and subsequently is closed to allow the data to recirculate in the loop. The storage capacity, i.e., amount of data stored, is limited by the time required to travel one loop τ_{loop} subtracted by that required to set the switch. This is because when the optical data stream is longer than τ_{loop}, the data of the leading part of the packets will overlap with that in the back to cause interference. The storage time, i.e., how long the data is kept in the loop, is an integer multiple of. The turn-off (release) time is also determined by τ_{loop}. This is because once a packet enters the delay line, it can only emerge at a fixed duration of time later. It is impossible to remove the packet from the delay line before that fixed time interval.

b. Slow Light Using Waveguide Dispersion:

Studies on the light propagation in highly dispersive structures with a very slow group velocity have drawn much attention. Grating structures have been used extensively in DFB lasers and grating waveguide couplers. Recent progress on the fabrication of grating structures in fiber has opened new research areas using fiber Bragg gratings [4]. Recently, another method for achieving slowed light based on a Moiré fiber Bragg grating has been suggested [5]. A Moiré grating is formed if the refractive index variation is given by

$$n(z) = n_0 + \delta n \cos(\frac{2\pi z}{\Lambda s}) \cos(\frac{2\pi z}{\Lambda}) \qquad\qquad (4\text{-}3)$$

where Λ is the Bragg period and Λs is the Moiré period. The theoretical analysis shows that the group velocity of light in the transmission band can be slowed down substantially although with a very small signal bandwidth.

c. Progress in EIT-Based Slow Light:

EIT refers to an artificially created spectral region of transparency in the middle of an absorption line due to the destructive quantum interference arising from two transitions in a three-level system [6], [7]. There are three basic energy level schemes for implementing a three-level EIT system interacting with two near-resonance electromagnetic fields. In a ladder or cascade system, levels are arranged as E1<E2<E3; in a V scheme, levels are arranged as E2<E1 and E3; whereas in a scheme, levels are arranged as E1, E3 <E2. In all three cases, we label the transitions the same way: |1> to |2>, and |2> to |3> are strong dipole-allowed transitions, while |1> to |3> is a dipole-forbidden transition.

The signal field connecting |1> to |2> is the light field that one desires to slow down in a controllable fashion. The pump field is the control field connecting |2> to |3>, whose intensity controls the amount of slowing down. In the literature, the pump laser is sometimes called the control laser.

As a result of the coherent coupling between the atomic system and the laser beams, atomic levels |1> and |2> are no longer eigenstates of the system. Instead, they are dressed by the pump laser and become two new states |2d> and |3d>. This (destructive) quantum interference between two absorption paths produces a transparency spectral window in the middle of the strong |1> to |2> absorption line. The width of this transparency window is strongly dependent on the intensity of the pump light field.

By the Kramers–Kronig relations, the induced transparency, which is related to the

imaginary part χ'' of the optical susceptibility χ, must be accompanied by a dispersive-shaped variation in the real part χ' of the susceptibility. Such a variation leads to a very large positive derivative (or gradient) of the index of refraction ($n \equiv \mathrm{Re}\sqrt{1+\chi}$) with respect to frequency inside the center of the EIT transparency region. This slope results in a very large group index of refraction and, thus, a reduced group velocity [8]–[10].

4.2 Tunable Slow Light Device of Quantum Dot VCSEL

4.2.1 Experimental Setup

The spectrum and LIV curve of the QD VCSEL in this experiment is shown in Fig. 4-1. The threshold current of the QD VCSEL is about 0.7mA. Fig. 4-2 shows the experimental setup for measuring the optical group delays in the QD VCSEL. A probe signal is generated by a tunable laser modulated with an electro-optical modulator. The OMI value of the modulated signal is about 50% and the signal is modulated at the linear region of the electro-optical modulator. The signal power is controlled by a variable optical attenuator at the output of the electro-optical modulator. The polarization of the tunable laser is adjusted by using a polarization controller before injecting into the QD VCSEL. The adjusted probe signal injects into the port 1 of optical circulator then passing into the QD VCSEL at the port 2.The light output at port 3 of optical circulator is divided into 2 parts: 90% of the light signal is transmitted into photo detector then convert into electrical signal amplified by RF amplifier and sent into oscilloscope to measure the delay condition. 10% of the light signal is connected to optical spectrum analyzer to observe the detuning wavelength of the probe signal and the QD VCSEL. The polarization of the probe signal is adjusted to reach the maximum time delay in the QD VCSEL.

4.2.2 Results and Discussion

Fig.4-3 shows the measurements of time delay for a 10 GHz probe signal at the various bias currents of QD VCSEL. The probe signal is tuned to the resonance of the QD VCSEL cavity, and the signal power is -14 dBm. Fig.4-4 is the cavity resonance dip at 0mA in 20^0C. The injection spectrum of QD VCSEL biased 1mA is shown as Fig.4-5. Increasing the bias current of QD VCSEL can increase the time delay of probe signal. The maximum group delay of 42 ps is observed, and the driving current is at 1 mA. The delay-bandwidth product is 0.42. Given the active region of 1.13μm this delay corresponds to the slow down factor of about 3280. Fig.4-6 shows the waveform at different modulation frequencies of probe signals when the bias current of QD VCSEL is at 1 mA. For 8 GHz and 6 GHz, the time delays are 44 ps and 60 ps, respectively, and the time-bandwidth product are 0.35 and 0.36, respectively. Moreover, the relationship between the time delays and modulation frequencies of probe signal are shown in Fig.4-7. The time delay in the QD VCSEL increases when the modulation frequency decreases. Fig.4-8 shows the waveform at different powers of probe signals when the bias current of QD VCSEL are at 1 mA and 0.6 mA. The time delays are 36 ps and 27 ps for -12 dBm and -10 dBm, respectively, when the bias current are at 1 mA. In addition, the time delays as a function of bias currents of QD VCSEL and optical power of probe signal are shown in Fig.4-9. We observe that the time delay increases as the signal power decreases.

4.3 Conclusion

We experimentally demonstrate tunable slow light using a 1.3 μm QD VCSEL at room temperature. Tunable optical group delays 42 ps for 10 GHz are achieved by varying the bias current, and the delay-bandwidth product is 0.42. This delay corresponds to the slow down factor of about 3280. Moreover, we also study that the relationship between the signal power and the tunable optical group delay.

Reference

[1] G. Lenz, B. J. Eggleton, C. K. Madsen, and R. E. Slusher, "Optical delay lines based on optical filters," *IEEE J. Quantum Electron.*, vol. 37, pp. 525–532, Apr. 2001.

[2] P. C. Ku, C. J. Chang-Hasnain, J. Kim, and S. L. Chuang, "Semiconductor all-optical buffers using quantum dots in resonator structures," in *Proc. OFC'03*, Atlanta, GA, Mar. 2003.

[3] R. Langenhorst, M. Eiselt, W. Pieper, G. Grosskopf, R. Ludwig, L. Kuller, E. Dietrich, and H. G. Weber, "Fiber loop optical buffer," *J. Lightwave Technol.*, vol. 14, pp. 324–335, Mar. 1996.

[4] K. O. Hill and G. Meltz, "Fiber Bragg grating technology fundamentals and overview," *J. Lightwave Technol.*, vol. 15, pp. 1263–1276, Aug. 1997.

[5] J. B. Khurgin, "Light slowing down in Moire fiber gratings and its implications for nonlinear optics," *Phys. Rev. A, Gen. Phys.*, vol. 62, p. 013 821, July 2000.

[6] S. E. Harris, "Electromagnetically induced transparency," *Phys. Today*, vol. 50, pp. 36–42, July 1997.

[7] J. P. Marangos, "Electromagnetically induced transparency," *J. Modern Opt.*, vol. 45, pp. 471–503, Mar. 1998.

[8] L. V. Hau, S. E. Harris, Z. Dutton, and C. H. Behroozi, "Light speed reduction to 17 meters per second in an ultracold atomic gas," *Nature*, vol. 397, pp. 594–598, Feb. 1999.

[9] D. F. Phillips, A. Fleischhauer, A. Mair, R. L.Walsworth, and M. D. Lukin, "Storage of light in atomic vapor," *Phys. Rev. Lett.*, vol. 86,

pp. 783–786, Jan. 2001.

[10] A. V. Turukhin, V. S. Sudarshanam, M. S. Shahriar, J. A. Musser, B. S. Ham, and P. R. Hemmer, "Observation of ultraslow and stored light pulses in a solid," *Phys. Rev. Lett.*, vol. 88, p. 023 602, Jan. 2002.
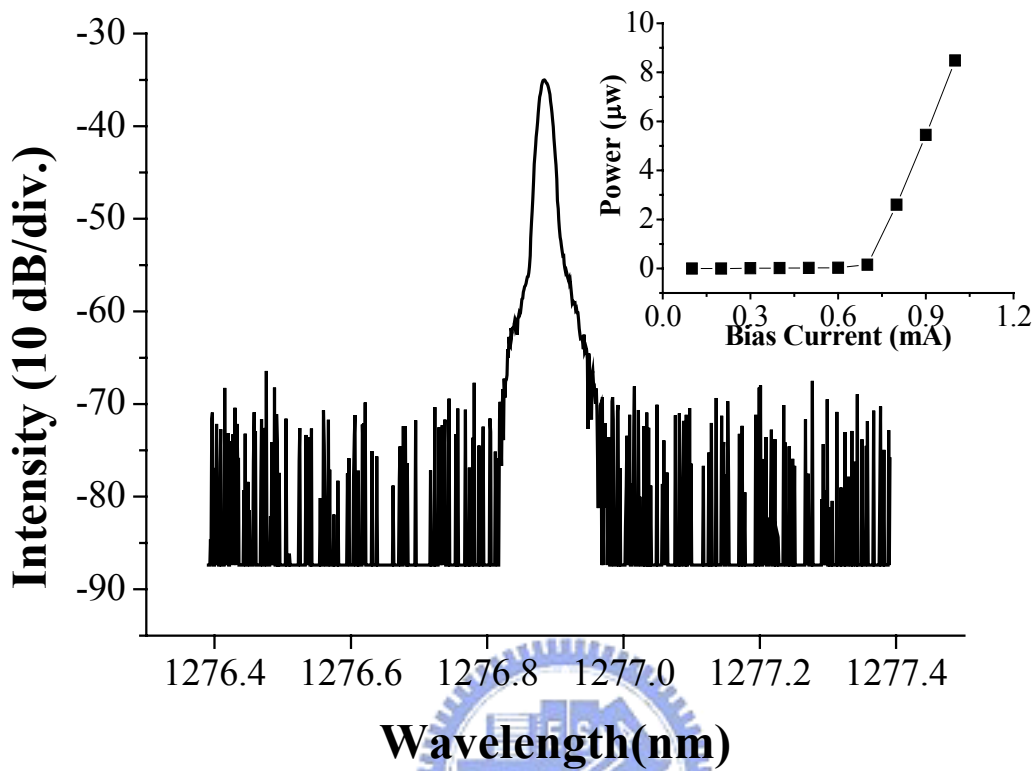
Fig.4-1. Optical spectrum and light-current characteristics of the QD VCSEL.
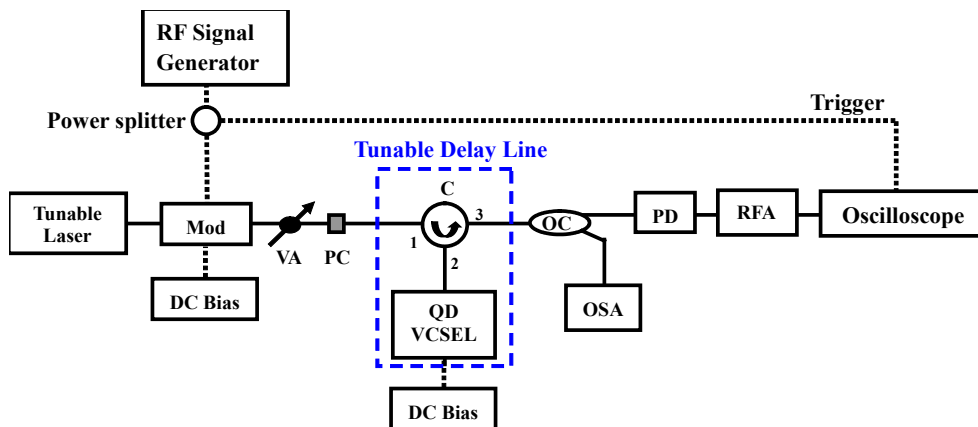

Fig.4-2. Experimental setup for measuring the optical group delays in QD VCSEL. (Mod: electro-optic modulator, VA: variable optical attenuator, C: optical circulator, OC: optical coupler, PC: polarization controller, RFA: RF amplifier, PD: photodetector, OSA: optical spectrum analyzer)
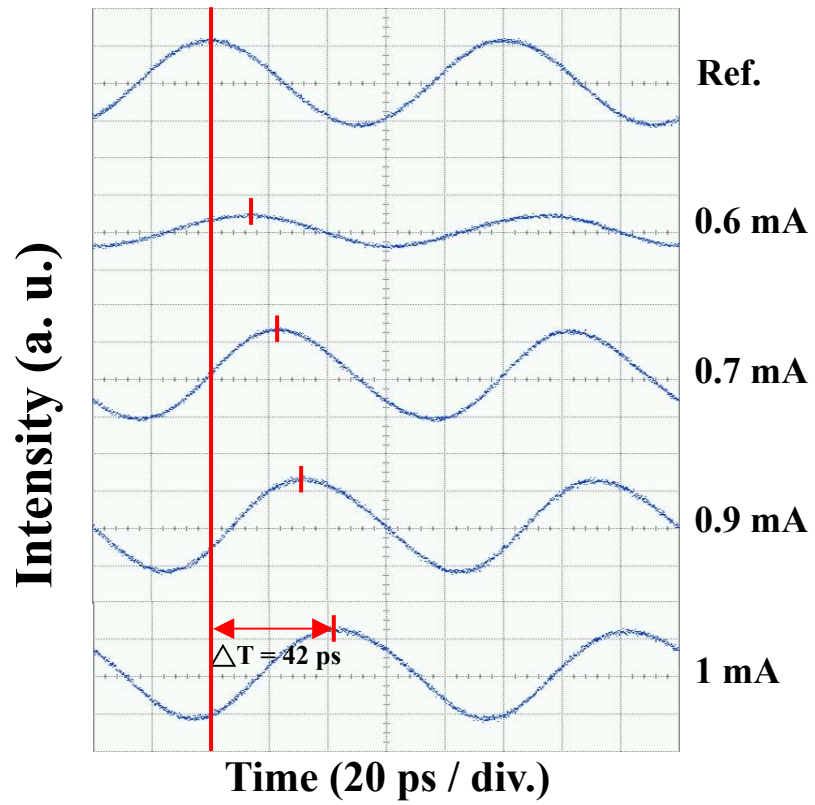
Fig.4-3. The measurements of time delay for a 10 GHz probe signal at the various bias currents of QD VCSEL.
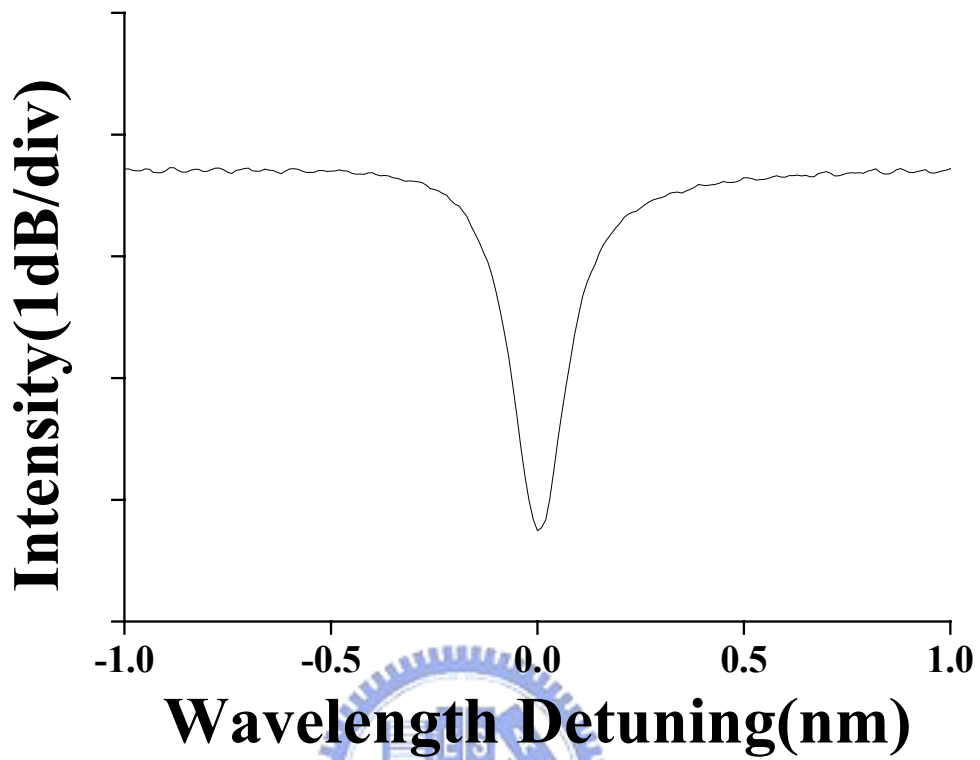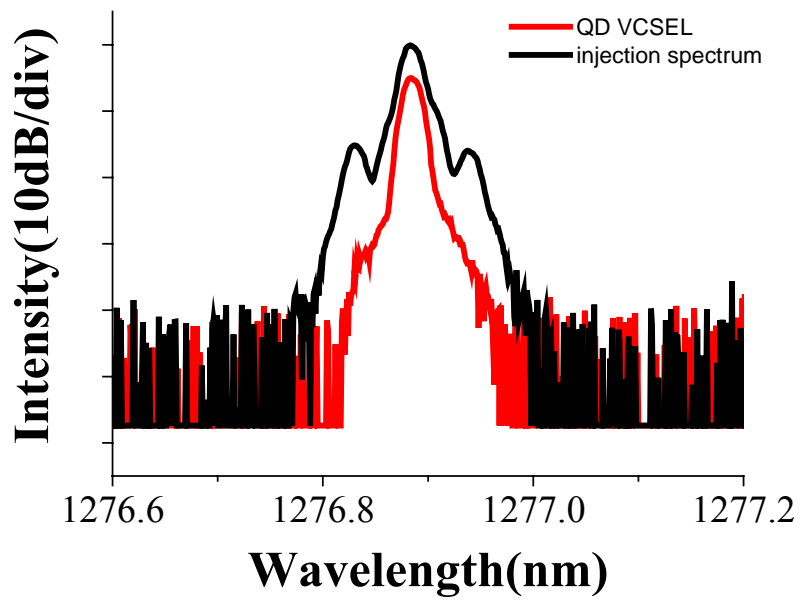
Fig.4-4. Absorption dip of QD VCSEL

Fig.4-5. Optical spectrum of tunable laser injecting into QD VCSEL

8 GHz

Ref.

1 mA

△T = 44 ps

Intensity (a. u.)

Time (20 ps / div.)

6 GHz

Ref.

1 mA

△T = 60 ps

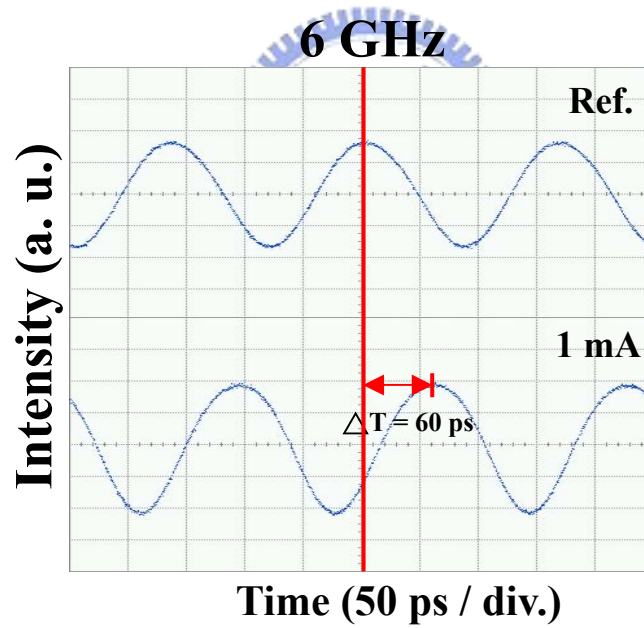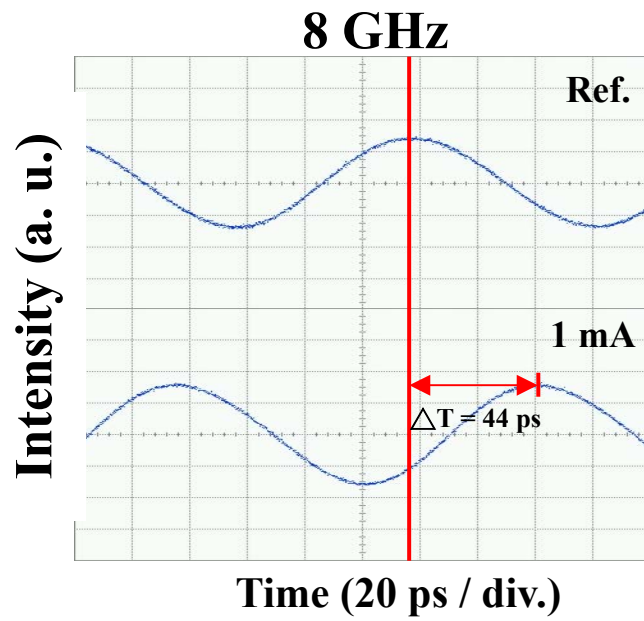Intensity (a. u.)

Time (50 ps / div.)

Fig.4-6. The waveform at different modulation frequencies of probe signals.

Fig.4-7. The relationship between the time delays and modulation frequencies of probe signals.
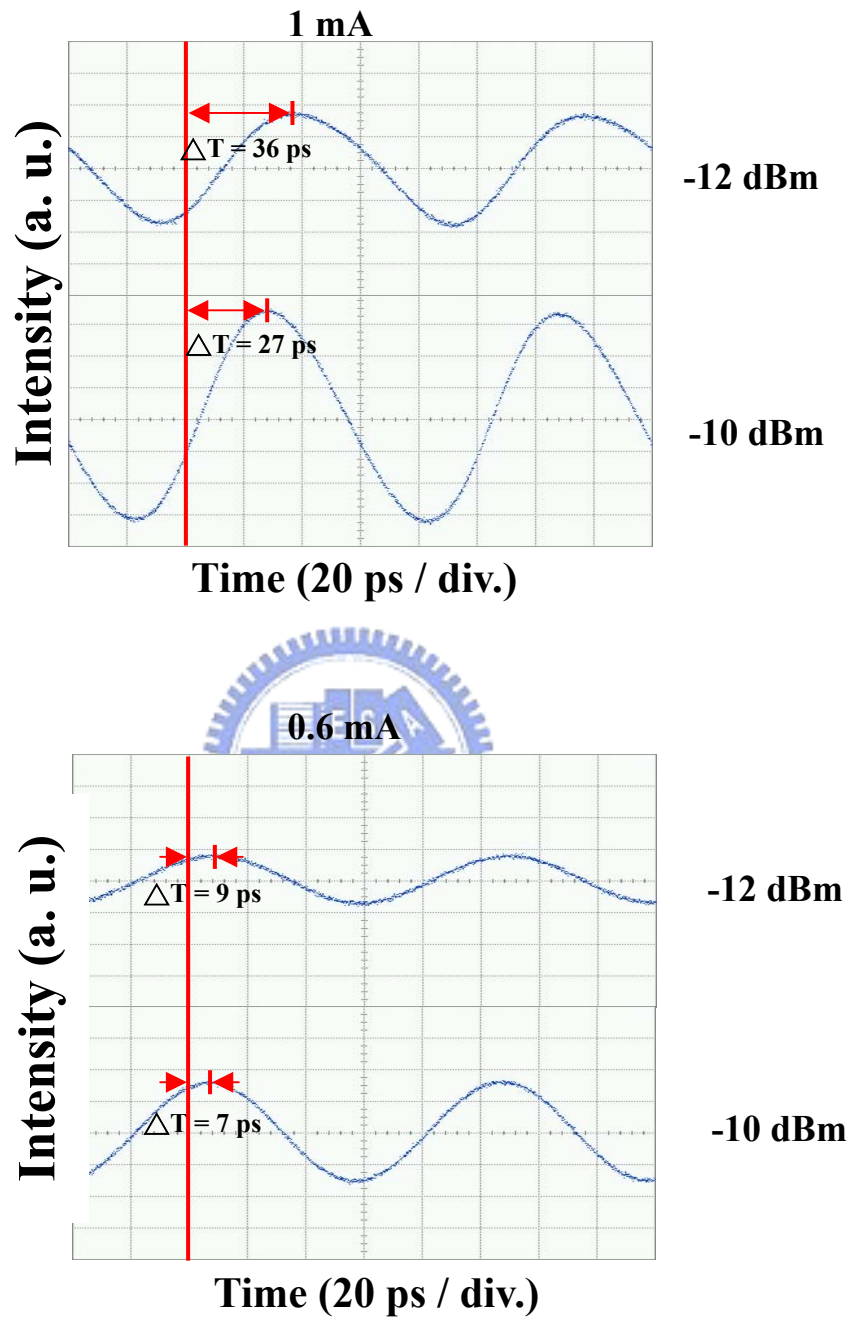
1 mA

Intensity (a. u.)

△T = 36 ps

-12 dBm

△T = 27 ps

-10 dBm

Time (20 ps / div.)

0.6 mA

Intensity (a. u.)

△T = 9 ps

-12 dBm

△T = 7 ps

-10 dBm

Time (20 ps / div.)
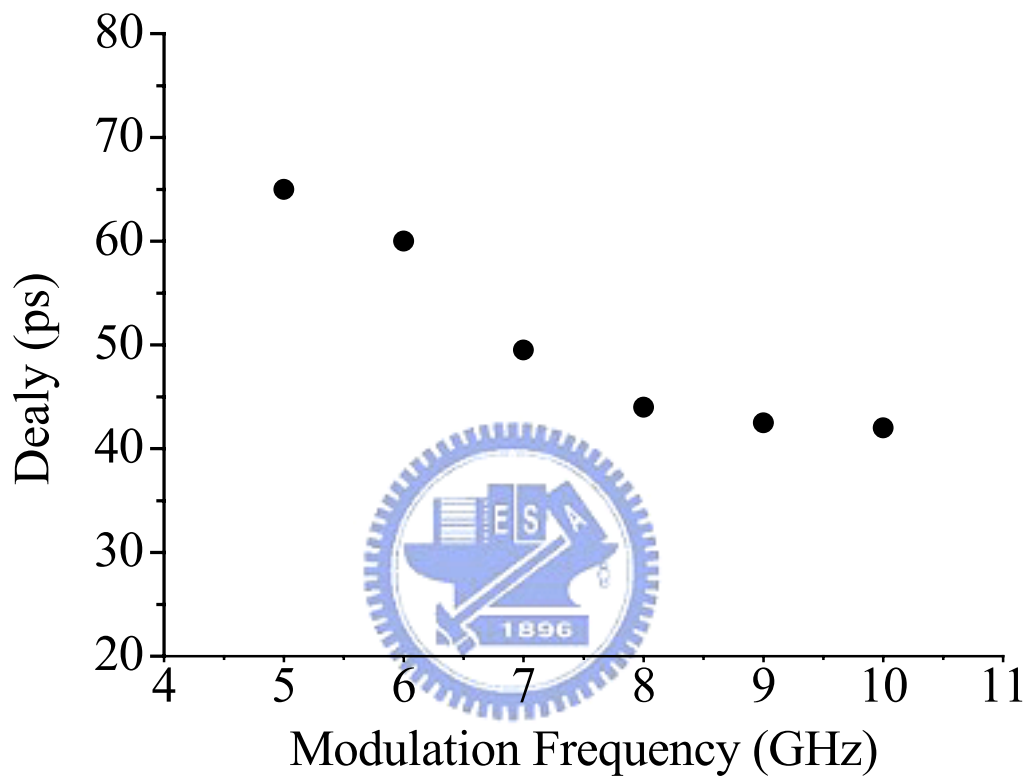
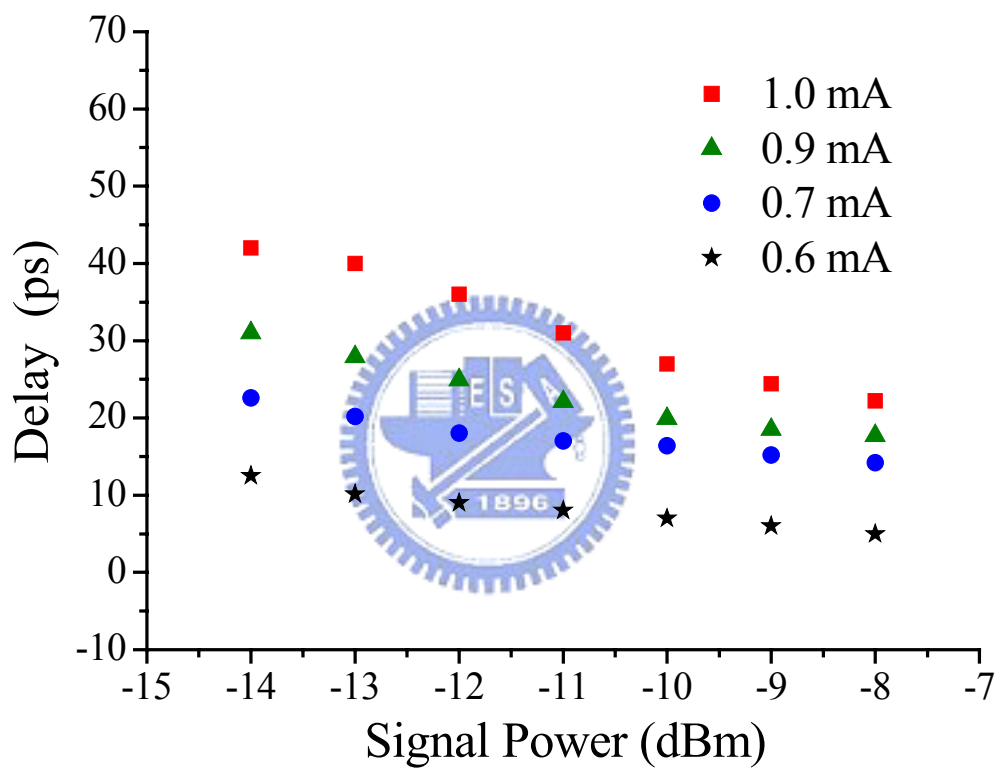**Fig.4-8.** The waveform at different powers of probe signals.

Fig.4-9. The time delays as a function of bias currents of QD VCSEL and optical power of probe signal.

Chap 5 Summary

5.1 Summary

In summary, we have studied high speed characteristics of quantum dot vertical-cavity surface-emitting laser. In Chapter 2, we demonstrate monolithically single-mode QD VCSELs with high side-mode suppression ratio. The QD VCSELs have adapted fully doped structure on GaAs substrate. The output power is ~ 330 μW with slope efficiency of 0.18 W/A at room temperature. Single mode operation was obtained with side-mode suppression ratio of > 30 dB. The high speed characteristics were also investigated. The free running bandwidth of QD VCSEL is ~2GHz. The modulation current efficiency factor (MCEF) is ~ 2.5 GHz/(mA)$^{1/2}$. Finally, we illustrate the eye diagram at 1.25 Gb/s and 2.5 Gb/s.

In Chapter 3, we report the experimental characterization of 1.3μm QD VCSEL with and without external light injection. Significant frequency response enhancement has been observed. The 3 dB frequency response has been increased by as much as 4.2 times using light injection technique. Furthermore, we demonstrate that this frequency response enhancement allows us to improve the performance of subcarrier multiplexed (SCM) system. A 33 dB improvement in systems performance is obtained with a SCM system for a 7-GHz 50-Mb/s data signal. We also report the third-order intermodulation distortion (IMD3) of QD VCSEL with and without external light injection. We observed that the dynamic range of the QD VCSEL with light injection can be enhanced 15.1 dB for the IMD3. These results show that external light injection is a very powerful technique to upgrade QD semiconductor lasers.

In Chapter 4, we report the slow light in the monolithically single-mode QD VCSEL. Tunable optical group delay can be achieved by adjusting the bias current. A 10 GHz modulation signal with tunable optical group delays 42 ps has been

demonstrated. The delay-bandwidth product is 0.42. We also study the relationship between the signal input power and the tunable optical group delay.

5.2 Future Work

Future work will be focus on the slow light in QD VCSEL. There will be some simulations about slow light mechanism of QD VCSEL. Further discussions on quantum dot medium and cavity resonance effect will be studied. Modulated laser signal with pseudo-random binary sequence (PRBS) data will pass the QD VCSEL to observe the delay condition.